Moisture origin as a driver of temporal variabilities of the water vapour isotopic composition in the Lena River Delta, Siberia

Jean-Louis Bonne[1], Hanno Meyer[2], Melanie Behrens[1], Julia Boike[2,3], Sepp Kipfstuhl[1], Benjamin Rabe[1], Toni Schmidt[2], Lutz Schönicke[2], Hans Christian Steen-Larsen[4], Martin Werner[1]

[1]Alfred-Wegener-Institut Helmholtz-Zentrum für Polar- und Meeresforschung, Bremerhaven, 27515 Germany
[2]Alfred-Wegener-Institut Helmholtz-Zentrum für Polar- und Meeresforschung, Potsdam, 14401, Germany
[3]Geography Department, Humboldt-Universität zu Berlin, Berlin, 10099, Germany
[4]Geophysical Institute, University of Bergen, and Bjerknes Centre for Climate Research, Bergen, 5020, Norway

Correspondence to: Jean-Louis Bonne (jean-louis.bonne@awi.de), Martin Werner (martin.werner@awi.de)

Abstract. In the context of the Arctic amplification of climate change affecting the regional atmospheric hydrological cycle, it is crucial to characterize the present-day's moisture sources of the Arctic. The isotopic composition is an important tool to enhance our understanding of the drivers of the hydrological cycle, due to the different molecular characteristics of water stable isotopes during phase change. This study introduces two years of continuous in situ water vapour and precipitation isotopic observations conducted since July 2015 in the east-Siberian Lena delta, at the research station on the Samoylov Island. The vapour isotopic signals are dominated by variations at the seasonal and synoptic time scales. Diurnal variations of the vapour isotopic signals are masked by synoptic variations, indicating low variations of the amplitude of local sources at the diurnal scale in winter, summer and autumn. Low amplitude diurnal variations in spring may indicate exchange of moisture between the atmosphere and the snow-covered surface. Moisture sources diagnostics based on semi-Lagrangian backward trajectories reveal that different air mass origins have contrasted contributions to the moisture budget of the Lena delta region. At the seasonal scale, the distance from the net moisture sources to the arrival site strongly varies. During the coldest months, no contribution from local secondary evaporation is observed. Variations of the vapour isotopic composition during the cold season on synoptic time scale are strongly related to moisture source regions and variations in the atmospheric transport: warm and isotopically-enriched moist air is linked with fast transport from the Atlantic sector; while dry and cold air with isotopically-depleted moisture is generally associated to air masses moving slowly over northern Eurasia.

1 Introduction

The amplitude of climate change in Arctic regions is likely to affect the atmospheric hydrological cycle, as sea ice is retreating and the temperatures are increasing, modifying the sources of evaporation and the saturation vapour pressure of the atmosphere. However, changes in evapotranspiration of Arctic regions during recent decades are poorly known, so far (Vihma et al., 2015).

Isotopic concentrations are commonly reported as $\delta^{18}O$ and $\delta^{2}H$, representing for the relative abundances of $H_2^{18}O$ and $H^2H^{16}O$, respectively, compared to the most abundant isotopologue $H_2^{16}O$. As isotope fractionation occurs during phase changes of water, they are largely used as tracers of the hydrological processes in the atmosphere and can be interpreted as proxies for past temperature variations in different types of climatic archives, such as ice cores, speleothems or ice wedges, specific ground ice features found in permafrost environments.

The $\delta^{18}O$ and $\delta^{2}H$ of precipitation and vapour at the global scale are primarily determined by the cooling-induced equilibrium distillation of the moisture from the source towards the measuring site. To the first order, this distillation affects both $H_2^{18}O$ and $H^2H^{16}O$ similarly, causing a global linear distribution of $\delta^{2}H$ versus $\delta^{18}O$ with a slope close to 8 (Craig, 1961). Additional phase change processes occurring during non-equilibrium, namely kinetic fractionation processes, such as fast evaporation from the ocean surface or snow crystals formation, are visible in deviations from this relationship (Dansgaard, 1964; Jouzel and Merlivat, 1984; Merlivat and Jouzel, 1979). To study the impacts of kinetic fractionation, the second order parameter deuterium excess, hereafter d-excess, has been defined as the deviation from this $\delta^{2}H$ to $\delta^{18}O$ relationship (Dansgaard, 1964).

Present-day observations of vapour and precipitation events refine the understanding of various phases of the atmospheric water cycle and their imprint on the water isotopic compositions (Galewsky et al., 2016). Such studies focus on exchange processes between the atmosphere and the Earth's surface, over open oceans (Benetti et al., 2014, 2017; Bonne et al., 2019; Zannoni et al., 2019), ice sheets (Madsen et al., 2019; Steen-Larsen et al., 2014), sea ice surfaces (Bonne et al., 2019), or continents (Bastrikov et al., 2014). Other studies focus on the atmospheric transport of moisture and show that typical vapour isotopic signals can be associated with distinct patterns of moisture origins (Bonne et al., 2014, 2015; Guilpart et al., 2017; Kopec et al., 2014; Steen-Larsen et al., 2013, 2015). However, the systematic relationship between water isotopes and atmospheric moisture transport remains uncertain in many conditions and locations. Recently, water vapour isotopic observations have also been showing great potential when used to benchmark the simulations of the hydrological cycle in General Circulation Models equipped with water isotopes (Steen-Larsen et al., 2017).

In the eastern Arctic region, water isotopic measurements of precipitation samples have been conducted at a land station along the Lena river (Zhigansk, 66.8°N, 123.4°E, 92 m above sea level) during multiple years (2004-2008) and have been combined with ship-based water vapour isotopic observations based on discrete samples during a campaign in the eastern Arctic Ocean on a period extending from before the sea-ice minimum to the beginning of the sea-ice growth season (Kurita, 2011). This study revealed that higher values of d-excess where observed at the land station in mid-Autumn for air masses originating from the Arctic Ocean region, compared to air masses originating from lower latitudes. A hypothesis to explain these high d-excess values was that evaporation over the ocean was taking place during the sea-ice growth season at very low relative humidity: the dry air masses originating from sea ice covered areas enhance evaporation with strong kinetic fractionation when passing over the open ocean.

More recently, continuous water vapour isotopic observations have been conducted in western Russia, at the Kourovka
observatory (Bastrikov et al., 2014; Gribanov et al., 2014) and at Labytnangy (Konstantin Gribanov and Jean Jouzel,
65 personal communication). Observations from the Kourovka station depicted seasonal and synoptic variations as well as
strong diurnal variations in summer on the first and second order vapour isotopic signals. To explain the lack of relationship
between vapour isotopic signal and meteorological parameters (humidity and temperature) in summer, a strong contribution
of continental recycling and local evapotranspiration has been suggested (Butzin et al., 2014). These observations were also
used to test the ability of an isotope-enabled Atmosphere General Circulation Model to reproduce the water vapour isotopic
70 composition and have shown an excellent correlation between simulation and water vapour δ^2H values measured at the
surface (Gribanov et al., 2014).

In this study, we focus on water vapour isotopic observations continuously performed from July 2015 to June 2017 at the
research station on Samoylov Island in Lena delta (72°22' N, 126°29' E), in the Russian Arctic. This station is at higher
latitude and much further east than the Kourovka and Labytnangy stations and will therefore be more representative of an
75 Arctic continental climate. We assess the variations of water vapour isotopic composition at different time scales, from the
seasonal to the synoptic and diurnal scales, and relate them with the variations of local meteorological parameters. In order
to interpret these variations in a larger regional context, we use atmospheric transport simulations together with moisture
source diagnostics. These simulations help to identify the main moisture advection regimes of the region and decipher the
imprint of local versus remote moisture sources on the locally observed water vapour isotopic composition.

80 ## 2 Method

2.1 Area of the study

The observations presented in this study have been conducted at the northeastern Siberian research station on the Samoylov
Island (72°22'N, 126°29'E), in the Lena river delta, extending over 150 km into the Laptev Sea. The island consists on its
western part of a flood plain and on its eastern part of a Holocene terrace characterised by polygonal tundra and larger
85 waterbodies. With a mean annual temperature below -12 °C, minimum winter air temperatures below -45 °C and summer air
temperatures that can exceed 25 °C, the region has a typical Arctic continental climate (Boike et al., 2013, 2019a). Average
annual rainfall is about 169 mm. The winter snow cover is thin (~0.3 m), with a maximum recorded of about 0.8 m in 2017.
The snow accumulation starts in late September and all the snow cover completely melts over a few days in early June.
Permafrost underlays the study area to depths between 400 and 600 m (Grigoriev, 1960), and the rate of permafrost
90 temperature warming at the zero annual amplitude niveau (ZAA) is one of the highest recorded (Biskaborn et al., 2019). The
active layer thawing period starts the end of May and active layer thickness reaches a maximum at the end of
August/beginning of September.

2.2 Meteorological observations

We used meteorological records from the Samoylov Island available from the PANGAEA database (Boike et al., 2019b),
95   conducted as part of a study focusing on the influence of meteorological parameters on the local permafrost evolution (Boike
et al., 2019a). The temporal resolution of this dataset in our period of interest is 30 minutes. The meteorological parameters
were measured at an approximate distance of 200 m eastward from our water isotopic observations. Here, we use the
following parameters always measured above the snow cover: relative humidity (RH, expressed in %) and air temperature
(expressed in °C), measured at 2 m above ground level; wind speed and wind direction (expressed in m s-1 and °), measured
100   at 3 m above ground level.

2.3 δ-notation for water isotopic compositions and d-excess

Isotopic compositions of samples are expressed as δ^{18}O and δ^{2}H in permille unit (‰). δ values are defined as (Craig, 1961):

$$\delta = 1000 \cdot \left(\frac{R_{sample}}{R_{VSMOW}} - 1 \right),$$ **(1)**

where δ can be either δ^{18}O or δ^{2}H, with R_{sample} and R_{VSMOW} as the isotopic ratios ($H_2^{18}O/H_2^{16}O$ or $H^2H^{16}O/H_2^{16}O$,
105   respectively) of the sample and the Vienna-Standard Mean Ocean Water (VSMOW) reference (Coplen, 2011).

We calculated the deuterium excess, noted d-excess using its classical definition (Dansgaard, 1964):

$$\text{d-excess} = \delta^2 H - 8.\delta^{18} O$$ **(2)**

2.4 Water isotopic observations (vapour and precipitation)

A Cavity Ring Down Spectrometer (CRDS) has been installed in July 2015 at the Samoylov station in order to continuously
110   record the near surface water vapour isotopic composition at an approximate 1 Hz frequency. The analyser is placed inside a
heated container and the ambient air inlet is located at 5 m above the ground level, above the roof of the container. The inlet
tube (1/4 inches diameter stainless steel tube of approximately 4 m length) is constantly heated at around 50°C. Following
the recommendations for long-term calibration of CRDS water vapour isotopic analysers (Bailey et al., 2015), a custom-
made calibration system allows the automatic correction of (i) the concentration-dependence of the isotopic measurements as
115   a function of the humidity level and (ii) the deviation from the Vienna Standard Mean Ocean Water (VSMOW2) (Coplen,
2011) scale on a daily basis. The system includes a custom-made vaporizer system(as described in Bonne et al., 2019)
allowing the measurement of four different water isotopic standards, and a bubbler system (similar to the one described in
Steen-Larsen et al., 2014) with one standard water of known isotopic composition. The data treatment and calibration
procedures are similar as for Bonne et al. (2019). Details on the calibration applied and the stability of the standards

120   measurements are given in the Supplementary Note 1. We note $\delta^{18}O_v$, δ^2H_v and d-excess$_v$ the isotopic values of the water
      vapour. Based on the uncertainty of both corrections of the concentration dependence and deviations from the VSMOW-
      SLAP scale, the measurement accuracy is estimated at 0.6‰, 3.0‰ and 5.7‰ on $\delta^{18}O_v$, δ^2H_v and d-excess$_v$. The
      measurement precision on 1-h averages, estimated from the standard deviation of calibration standard measurements at a
      constant humidity level, is of 0.25‰, 0.5‰ and 2‰ on $\delta^{18}O_v$, δ^2H_v and d-excess$_v$ for humidity levels above 3 g/kg. It

125   deteriorates logarithmically with lower humidity levels, reaching 2.0‰, 6.5‰ and 17‰ for $\delta^{18}O_v$, δ^2H_v and d-excess$_v$, for
      humidity levels of 0.3 g/kg. The dataset presented in this study has been averaged at a 6-h temporal resolution (except for the
      calculation of the diurnal cycle based on the hourly averaged dataset) and the precision can therefore be estimated at 0.10‰,
      0.2‰ and 1‰ on $\delta^{18}O_v$, δ^2H_v and d-excess$_v$ for humidity levels above 3 g/kg and 0.8‰, 2.7‰ and 7‰ for $\delta^{18}O_v$, δ^2H_v and d-
      excess$_v$, for humidity levels of 0.3 g/kg.

130   Technical difficulties linked with the extreme cold and dry conditions during winter and the remote location of the station
      lead to some periods of missing data. Modifications of the instrumental setup and calibration procedure during the successive
      maintenance expeditions allowed to progressively enhance the precision of the measurements.

**2.5 Water isotopic composition of event-based precipitation samples and calculation of equilibrium vapour isotopic
composition**

135   Event-based precipitation samples retrieved over the period of the study have been measured for their water isotopic
      composition in the stable isotope laboratory of the Alfred Wegener Institute, Helmholtz Centre for Polar and Marine
      Research, in Potsdam. Isotope ratios were determined by isotope ratio mass spectrometry using a Finnigan MAT Delta-S
      mass spectrometer, applying the equilibration technique (Meyer et al., 2000). The measurement accuracy is better than 0.1
      ‰ for $\delta^{18}O_p$ and 0.8 ‰ for δ^2H_p (Meyer et al., 2000). We note $\delta^{18}O_p$, δ^2H_p and d-excess$_p$ the isotopic values of precipitation.

140   To compare the vapour and precipitation isotopic dataset, we calculate the isotopic composition of a theoretical water vapour
      at equilibrium with the precipitation, from the measured $\delta^{18}O_p$ and δ^2H_p values. We use the α_{eq} equilibrium fractionation
      coefficients between liquid (solid) and vapour for air temperatures above (below) the freezing point (Majoube, 1971a,
      1971b; Merlivat and Nief, 1967). For each precipitation sample, with an isotopic ratio denoted R_P, the theoretical isotopic
      ratio of vapour, denoted R_V, is given by $R_V = R_P/\alpha_{eq}$.

145   **2.6 Selection of synoptic extrema from meteorological and vapour isotopic parameters**

      We identify the extrema occurring at a synoptic time scale for a set of parameters based on the daily averaged dataset:
      temperature, logarithm of the specific humidity, $\delta^{18}O_v$ and d-excess$_v$. We use the logarithm of specific humidity for
      comparability regarding its logarithmic relationship with temperature (Clausius-Clapeyron relationship). For each parameter,

we compute the distances of the daily values to a 60-days running average and identify the extrema as the first and last

150   deciles of this dataset (low and high extrema, respectively). As some data gaps exist at different periods for the temperature, specific humidity and the isotopic parameters, we use only data with simultaneously valid measurements for all parameters to be certain that the selection of the events for all the parameters cannot be affected by different sampling times.

2.7 Sea ice cover data

The sea ice coverage within the 500 km area surrounding the station has been derived from ERA-interim reanalyses (Dee et

155   al., 2011) at 0.75° × 0.75° spatial and 6-h temporal resolution. Results are shown as a proportion of sea ice covered surface compared to the surface of the surrounding 500 km area. As this area includes grid cells covered by land, the maximum value is lower than 1.

2.8 Moisture source diagnostics

The origin of the moisture arriving at our research area is estimated using a moisture source diagnostics method (Sodemann

160   et al., 2008) based on semi-Lagrangian simulations of air masses transport with the model FLEXPART version 8.1 (Stohl et al., 2005). Meteorological fields from the ECMWF ERA-interim dataset (Dee et al., 2011) at 0.5° horizontal resolution and 137 vertical levels are used. Air parcels are traced 10 days backward in time from a box centred around the Samoylov station. The box has a 3°x6° latitudinal and longitudinal width and spans altitudes between 0 and 500 m. All simulation outputs are presented over a global grid of 1°x1° resolution representing the summed contribution of all individual particles.

165   From the air mass trajectory simulations, without considering the transport of moisture yet, we calculate the parameter "trajectories locations", as the summed number of air masses passing within each grid cell over all time steps. This parameter is representative of the location of transported air masses.

As different air masses can carry various amounts of moisture, a complementary calculation is conducted to properly evaluate the atmospheric transport of moisture: this moisture source diagnostics consists of interpreting the increase or

170   decrease of the moisture content of air masses between different successive time steps along their trajectories respectively as an input or output of moisture contributing to the total moisture at the end of the trajectories. The contribution of every single air mass in terms of input and output of moisture is summed over all model output grid cells. Different parameters are estimated over this grid. The parameter "moisture uptake" (expressed in mm/day) represents the amount of moisture injected to the air masses within each grid cell. Moisture uptakes are interpreted as evaporation, transpiration or sublimation at the

175   surface when the air masses are below an altitude equal to 1.5 times the boundary layer height. Moisture uptakes are interpreted as the result of mixing of different air masses or reevaporation of falling precipitation when the air masses are above this threshold, therefore within the free troposphere (Dütsch et al., 2017). Therefore, the parameters "boundary layer moisture uptake" and "free troposphere moisture uptake" are presented separately. The parameter "evaporation minus

precipitation" (expressed in mm/day) represents the sum of the differences between the moisture uptakes and moisture losses
180   of all particles occurring in each grid cell.

3 Results

3.1 Ranges of variations of isotopic and meteorological dataset

Over the observational period (2015-07-01 to 2017-07-01), the dataset comprises a total of 2395 water vapour isotopic
values, at a 6-hours resolution. All observed parameters, presented in Figure 1, are characterized by variations at the
185   interannual, seasonal, synoptic and eventually diurnal timescales.

For temperature and specific humidity distributions, the amplitude of seasonal variations is larger than the amplitude of
synoptic variations (Figure 1). The complete observation period presents averages of specific humidity and temperature of
2.4 g kg^{-1} and -11 °C (Table 1). Minimal and maximal temperatures reach -41.1 °C and +21.5 °C, respectively (Table 1).
This two-years period is not exceptional, as observations over 16-years on this site have recorded temperature extremes
190   below -45 °C and above +25 °C, with an average mean annual temperature of -12 °C (Boike et al., 2019a), close to the
average on our observational period. Specific humidity values reach extremely dry values in winter, down to 0.06 g kg^{-1}, and
maximum values in summer up to 12 g kg^{-1}. A non-linear distribution between air temperature and specific humidity is
observed (Figure 2b), as expected from the Clausius-Clapeyron relationship. Relative humidity values vary between 40%
and 102%, with a mean value of 84% (Table 1).
195   Important local hydrological changes are expected between evapotranspiration or sublimation-dominated regimes during the
warm and the cold seasons. The surroundings of the station are indeed characterised by contrasted surface covers between
these seasons, with ice-free or ice-covered Lena river, land areas covered by vegetation or snow and the surrounding Laptev
Sea covered by sea ice during the cold season. Locally measured snow depth indicates the permanent presence of a snow
cover from the last days of September to June. Melting takes place within a few days, until mid-June (in 2016) or end of
200   June (in 2017), as seen on Figure 1. Satellite images from the MODIS sensor on the Terra satellite reveal that ice covering
the river in the Lena delta completely disappears within a few days, between May 23rd and June 10th in 2016 and between
May 29th and June 13th in 2017. The freeze-up of the Lena river also takes place within a few days and has been estimated
between October 10^{h} and 20th in 2015 and between October 15th and 22nd in 2016. The sea ice cover on the Laptev sea, as
estimated from the proportion of sea ice within the surrounding 500 km derived from the ERA-interim data, also depicts the
205   fast opening of polynya in early June (Figure 1). Presence of a significant sea ice cover in the region is still observed in July
and the complete disappearance of sea ice occurs by the end of August. The complete sea ice cover then builds up within a
few weeks in October (in mid-October in 2015 and in the second half of October in 2016). All these different surface cover
changes take place simultaneously and within a few days or weeks in autumn and spring. It is therefore difficult to
investigate the impact of the change of each potential local moisture source individually.

For $\delta^{18}O_v$ and δ^2H_v, some episodes of winter synoptic variations reach almost the amplitude of the seasonal cycle, while the d-excess$_v$ signal is predominated by synoptic variations (Figure 1). The vapour $\delta^{18}O_v$, δ^2H_v and d-excess$_v$ have averaged values over the complete dataset of respectively -36.9‰, -270‰ and 24.6‰ (Table 1). Water vapour isotopic composition minima and maxima are -53.2‰ and -20.9‰ for $\delta^{18}O_v$, -382‰ and -155‰ for δ^2H_v and 3‰ and +62‰ for d-excess$_v$. At Samoylov, the $\delta^{18}O_v$ and δ^2H_v are overall strongly correlated, with the following empirical relationship:

$\delta^2H_v = 7.2 \times \delta^{18}O_v - 6.7$, $R^2 = 0.98$ (Figure 2.a). This slope is a little lower than the slope of 7.5 obtained from observations at the Kourovka observatory in western Siberia (Bastrikov et al., 2014) and lower than the LMWL of Samoylov precipitation (LMWL: $\delta D = 7.6\ \delta^{18}O - 5.5$ (n = 208, $R^2 = 0.95$, p < 0.05). While the warm seasons isotopic compositions are similar between both years, significant differences between the average d-excess$_v$ values during the cold seasons are noticed, with higher d-excess$_v$ values during winter and spring 2016 than in 2017 (average and standard deviations on d-excess$_v$ of +32.5 ‰ +/- 9.0 ‰ from December 2015 to April 2016 and of +22.7 ‰ +/- 7.5 ‰ from December 2016 to April 2017).

The precipitation samples also depict interannual, seasonal and synoptic time scale variations. Altogether, precipitation samples depict more enriched δ-values and lower d-excess than vapour, with mean values over the complete observation period for $\delta^{18}O_p$, δ^2H_p and d-excess$_p$ of respectively -21.6‰, -169.3‰ and 3‰ (Table 1). The difference between vapour and precipitation is stable throughout all seasons for δ-values, but is varying between seasons for the d-excess with higher gaps in spring (maximum gap) and winter than in summer (minimum gap) and autumn. Precipitation samples have on average 14.5‰ lower d-excess values than vapour in summer and 28.5‰ lower d-excess values in spring, as shown in Table 1. Significant interannual variations are noticed during the cold seasons on the values of $\delta^{18}O_p$ and δ^2H_p and particularly on d-excess$_p$, with higher $\delta^{18}O_p$ and δ^2H_p and lower d-excess$_p$ values during winter and spring 2016 than in 2017 (average and standard deviations on $\delta^{18}O_p$ and d-excess$_p$ respectively of -24.7 ‰ +/- 5.4 ‰ and -9.1 +/- 17.8 ‰ from December 2015 to April 2016 and of -29.2 ‰ +/- 5.2 ‰ and +9.5 ‰ +/- 7.7 ‰ from December 2016 to April 2017). The difference in precipitation d-excess$_p$ levels between both years is in the opposite direction compared to the difference observed in the vapour d-excess$_v$.

The minima of specific humidity are associated with the lowest $\delta^{18}O_v$ and δ^2H_v and the highest d-excess$_v$ values, comparable to vapour observations performed on the East Antarctic Plateau in summer (Casado et al., 2016; Ritter et al., 2016). This could indicate a strong isotopic depletion during long-range atmospheric transport from the moisture sources to the location of the observations, or recycling of moisture with sublimation over the surrounding snow-covered areas (Pang et al., 2019). Such high d-excess$_v$ values do not only reflect kinetic fractionation processes, but are also partly due to the variations of the $\delta^{18}O_v$ to δ^2H_v relationship during equilibrium fractionation at very low temperatures (Dütsch et al., 2017).

There is a linear relationship between $\delta^{18}O_v$ and air temperature (with a slope of 0.44‰ °C^{-1}, R^2=0.75, p< 0.01, Figure 2.c), but with a large scatter clearly demonstrating that the air temperature variations do not fully explain the $\delta^{18}O_v$ variations. This linear relationship observed in vapour is close to the 0.4 ‰ °C^{-1} relationship obtained both for local precipitation $\delta^{18}O_p$ on event and monthly means, as well as for $\delta^{18}O_v$ and T in the west Siberian Kourovka station. A non-linear relationship

between $\delta^{18}O_v$ and specific humidity is also depicted (Figure 2.d). We note for low temperatures and specific humidity values (below -20°C and 0.1 g/kg) that the distribution of $\delta^{18}O_v$ values against temperature and specific humidity is curved towards higher $\delta^{18}O_v$ values, compared to this linear relationship. It is not certain if this deviation can be attributed to an atmospheric process (such a more important relative contribution of additional moisture sources at very low humidity compared to higher humidity levels), or if is due to a remaining observational bias or contamination that could not be identified despite our calibration and flagging processes.

Season		T (°C)	q (g/kg)	RH (%)	$\delta^{18}O_v$ (‰)	$\delta^{18}O_p$ (‰)	δ^2H_v (‰)	δ^2H_p (‰)	d-excess$_v$ (‰)	d-excess$_p$ (‰)
Winter (DJF)	Mean	-29.3	0.32	77.5	-44.0	-30.0	-325.2	-237.9	27.2	1.9
	St. dev.	5.9	0.22	6.3	3.6	4.8	26.0	33.9	9.4	12.0
	Min.	-40.9	0.06	60.6	-52.6	-41.3	-378.2	-324.6	2.6	-39.7
	Max.	-8.23	2.20	93.9	-32.9	-12.5	-244.6	-140.0	53.3	15.6
	N	684	620	724	550	43	550	43	550	43
Spring (MAM)	Mean	-14.7	1.48	86.0	-40.4	-24.4	-294.9	-195.7	28.1	-0.4
	St. dev.	9.4	0.98	6.2	5.3	5.3	35.7	35.5	9.8	19.5
	Min.	-41.1	0.06	66.1	-53.2	-36.8	-381.8	-291.3	9.0	-56.1
	Max.	3.5	4.63	101.2	-27.0	-8.7	-203.9	-108.3	62.1	33.1
	N	736	661	736	650	46	650	46	650	46
Summer (JJA)	Mean	6.9	5.56	83.7	-28.8	-15.9	-211.3	-122.2	19.1	4.6
	St. dev.	4.6	1.61	10.5	2.6	2.4	19.1	18.1	5.9	6.8
	Min.	-4.9	2.41	40.3	-36.7	-21.7	-274.1	-166.0	6.7	-12.2
	Max.	21.5	11.99	101.4	-20.9	-10.1	-155.3	-83.9	37.8	15.2
	N	748	583	748	577	61	577	61	577	61
Autumn (SON)	Mean	-8.6	2.41	88.3	-34.3	-19.1	-250.7	-147.4	23.9	5.7
	St. dev.	11.6	1.90	7.4	7.2	6.2	50.4	45.2	9.4	11.4
	Min.	-37.4	0.12	61.0	-53.1	-31.1	-370.5	-252.8	4.3	-60.9
	Max.	17.6	8.95	101.9	-20.8	-2.3	-162.4	-79.3	56.1	19.6
	N	728	618	726	618	59	618	59	618	59
All	Mean	-11.0	2.28	83.9	-36.9	-21.6	-270.3	-169.3	24.6	3.3
	St. dev.	15.4	2.33	8.8	7.6	7.1	55.1	55.6	9.5	13.0
	Min.	-41.1	0.06	40.3	-53.2	-41.3	-381.8	-324.6	2.6	-60.9
	Max.	21.5	11.99	101.9	-20.8	-2.3	-155.3	-79.3	62.1	33.1
	N	2896	2482	2934	2395	209	2395	209	2395	209

250 **Table 1: Averaged values, standard deviations, minima, maxima and number of values for all seasons and for the whole dataset within the period 2015-07-01 to 2017-06-30, with 6 hours averaged dataset, for air temperature (°C), specific humidity q (/kg), relative humidity (%), $\delta^{18}O_v$ (‰), $\delta^{18}O_P$ (‰), δ^2H_v (‰), δ^2H_P (‰) d-excess$_v$ (‰) and d-excess$_p$ (‰).**
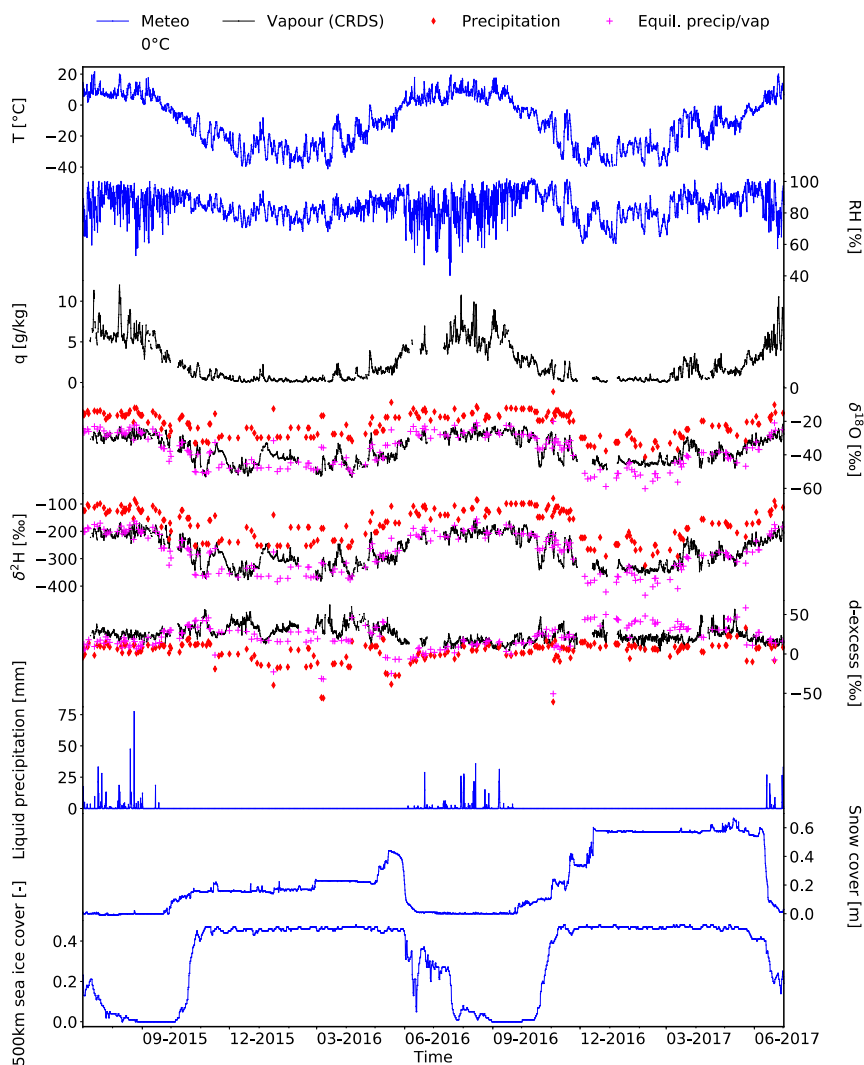
Figure 1: Time series of ambient air observations at Samoylov for the period 2015-07-01 to 2017-07-01 at 6 hours temporal resolution for air temperature (°C), relative humidity (%), specific humidity q (g kg^{-1}), δ^{18}O$_v$ (‰), δ^{2}H$_v$ (‰) and d-excess$_v$ (‰), liquid precipitation amount (mm), depth of the snow cover (m) and proportion of the area within 500 km around the station which is covered by sea ice. Plain blue lines indicate the continuous parameters recorded from the meteorological station. Plain black lines depict the continuous measurements of the water vapour analyser. Red diamonds represent the discrete isotopic measurements from the snow samples. Purple crosses represent the theoretical vapour isotopic composition, calculated from precipitation isotopic composition considering equilibrium fractionation. For the temperature, the 0°C line is indicated by a plain horizontal grey line.
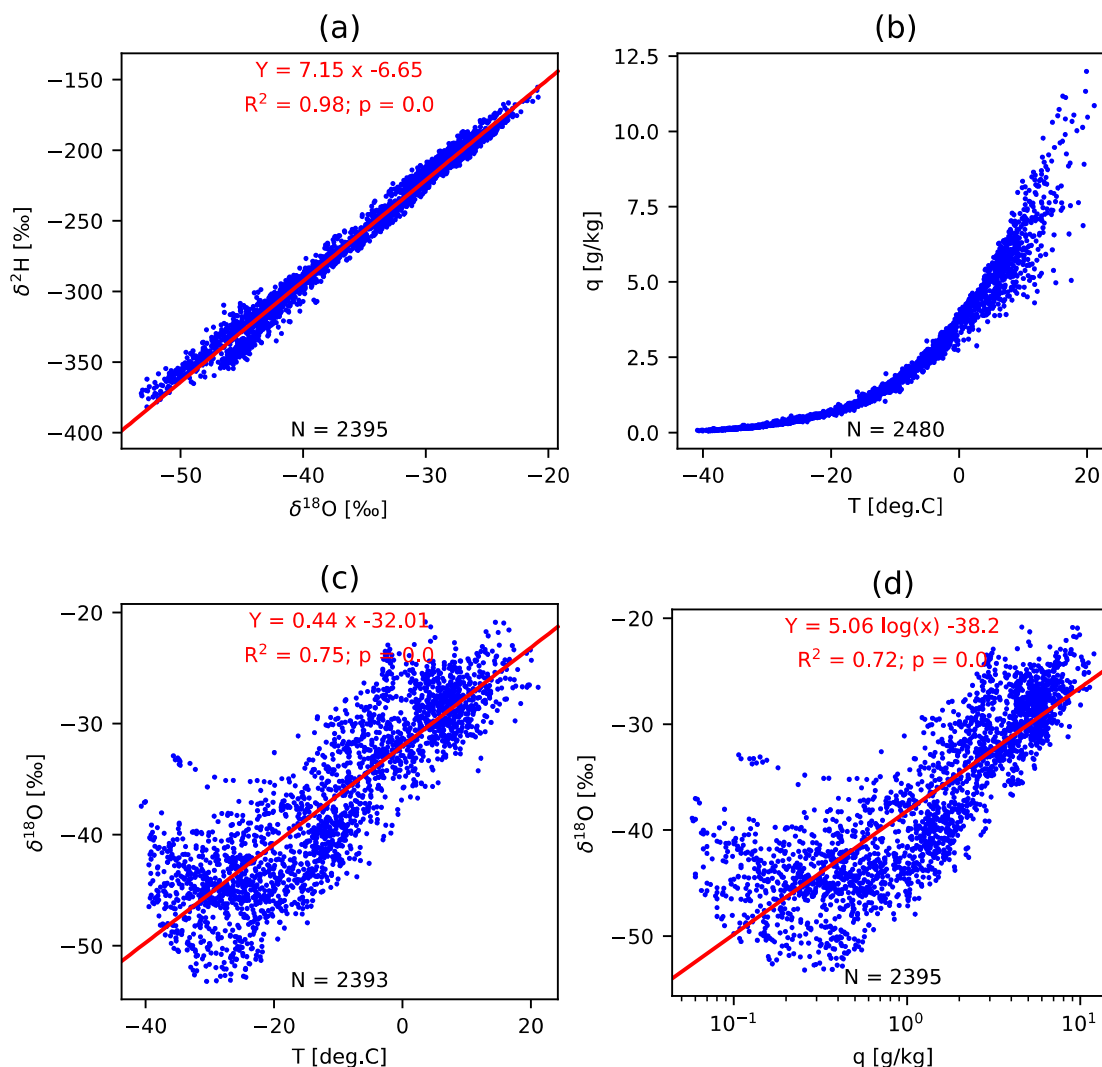
Figure 2: Covariations of water vapour isotopic composition and meteorological parameters, for the complete period 2015-07-01 to 2017-07-01. Red lines represent the best estimate of the linear regression.

3.2 Seasonal cycle

A clear average seasonal cycle is observed (Figure 3 and Table 1) for temperature, specific humidity and relative humidity as well as for the water vapour isotopic composition (δ_v-values and d-excess$_v$). The δ^2H seasonal variations (not shown) are very similar to the $\delta^{18}O_v$ seasonal variations (correlation coefficient R^2 =1.0, p<0.01, with a slope of 7.34 considering the monthly averages). At the first order, the temperature depicts similar variations than the δ_v-values, with a maximum during

summer compared to winter ($\delta^{18}O_v$/T slope of 0.45‰ °C^{-1} considering the monthly averages, R^2 =0.92, p<0.01, Figure 3 and Table 2).

A summer peak of temperature and specific humidity is reached in July (monthly averaged values of +8.1°C and 6.1 g/kg). Significantly colder and drier specific humidity conditions are already measured in September (about +3.6°C and 4.6 g/kg

275   lower). For δ_v-values however, a plateau of maximal values is extending from July to September, with monthly mean $\delta^{18}O_v$ values of -28‰.

For the studied period, the lowest temperatures are measured in December, January and February (with respective monthly means of -30.1°C, -27.1°C and -30.7°C). Very dry air is observed during whole winter (specific humidity below 1 g/kg from November to February, with two minima at 0.26 and 0.30 g/kg in February and December, respectively). Interestingly, the

280   minimum monthly averaged $\delta^{18}O_v$ values are observed in December (-47.1‰) and not in February (-44.1‰), while February is the coldest and driest month. This is also true when considering only the data for which all meteorological and vapour isotopic data are simultaneously available (not shown here) and therefore not due to a bias linked with different sampling periods.

Transitions between the summer and winter regimes are observed for temperature, specific humidity and $\delta^{18}O_v$ in March to

285   June for spring and September to November for autumn. We note a temperature, humidity and $\delta^{18}O_v$ increase at the beginning of March (+10.5°C, +0.8 g/kg and +2.7‰ difference in monthly average between February and March), stagnant until mid-April, before a sharp increase towards summer values until July. This increase of the monthly average values of temperature, specific humidity and $\delta^{18}O_v$ in March is accompanied by a large temporal variability compared to the winter months (Figure 3). This suggests that this early-spring transition is primarily linked with an increase of the synoptic

290   variability.

Month	T (°C)	q (g/kg)	RH (%)	$\delta^{18}O_v$ (‰)	δ^2H_v (‰)	d-excess$_v$ (‰)
January	-27.1 +/- 5.1	0.41 +/- 0.,3	79.2 +/- 6.6	-41.5 +/- 3.2	-308.6 +/- 26.3	23.3 +/- 5.9
February	-30.7 +/- 5.5	0.26 +/- 0.2	77.2 +/- 5.3	-44.1 +/- 2.3	-329.2 +/- 21.4	23.4 +/- 8.9
March	-20.2 +/- 10.6	1.04 +/- 0.9	83.5 +/- 6.9	-41.4 +/- 5.8	-305.9 +/- 39.4	25.5 +/- 10.4
April	-15.8 +/- 7.6	1.31 +/- 0.9	85.4 +/- 4.9	-41.4 +/- 5.6	-298.8 +/- 36.8	32.7 +/- 9.3
May	-8.3 +/- 4.8	2.04 +/- 0.9	89.2 +/- 5.0	-38.6 +/- 4.0	-281.2 +/- 25.0	27.3 +/- 8.2
June	4.7 +/- 4.9	4.55 +/- 1.5	83.1 +/- 10.3	-30.3 +/- 2.6	-226.6 +/- 19.0	15.9 +/- 3.2
July	8.1 +/- 4.2	6.1 +/- 1.4	82.8 +/- 11.5	-28.5 +/- 2.2	-207.4 +/- 14.2	20.5 +/- 7.6
August	7.9 +/- 3.6	5.9 +/- 1.5	85.2 +/- 9.5	-28.0 +/- 2.4	-203.6 +/- 15.8	20.2 +/- 5.2
September	3.6 +/- 5.3	4.6 +/- 1.6	88.6 +/- 8.2	-28.3 +/- 3.4	-207.5 +/- 22.0	18.9 +/- 7.3
October	-8.7 +/- 4.8	1.9 +/- 0.8	91.6 +/- 5.0	-34.3 +/- 6.4	-250.2 +/- 44.3	24.0 +/- 8.9
November	-20.8 +/- 7.5	0.8 +/- 0.6	84.6 +/- 6.9	-40.2 +/- 5.8	-293.2 +/- 38.6	28.5 +/- 9.3
December	-30.1 +/- 6.0	0.3 +/- 0.2	76.2 +/- 6.4	-47.1 +/- 2.5	-341.2 +/- 16.1	35.2 +/- 8.3

Table 2: Monthly averaged values and standard deviations for the period 2015-07-01 to 2017-06-30, for air temperature (°C), specific humidity q (/kg), relative humidity (%), $\delta^{18}O_v$ (‰), δ^2H_v (‰) and d-excess$_v$ (‰).
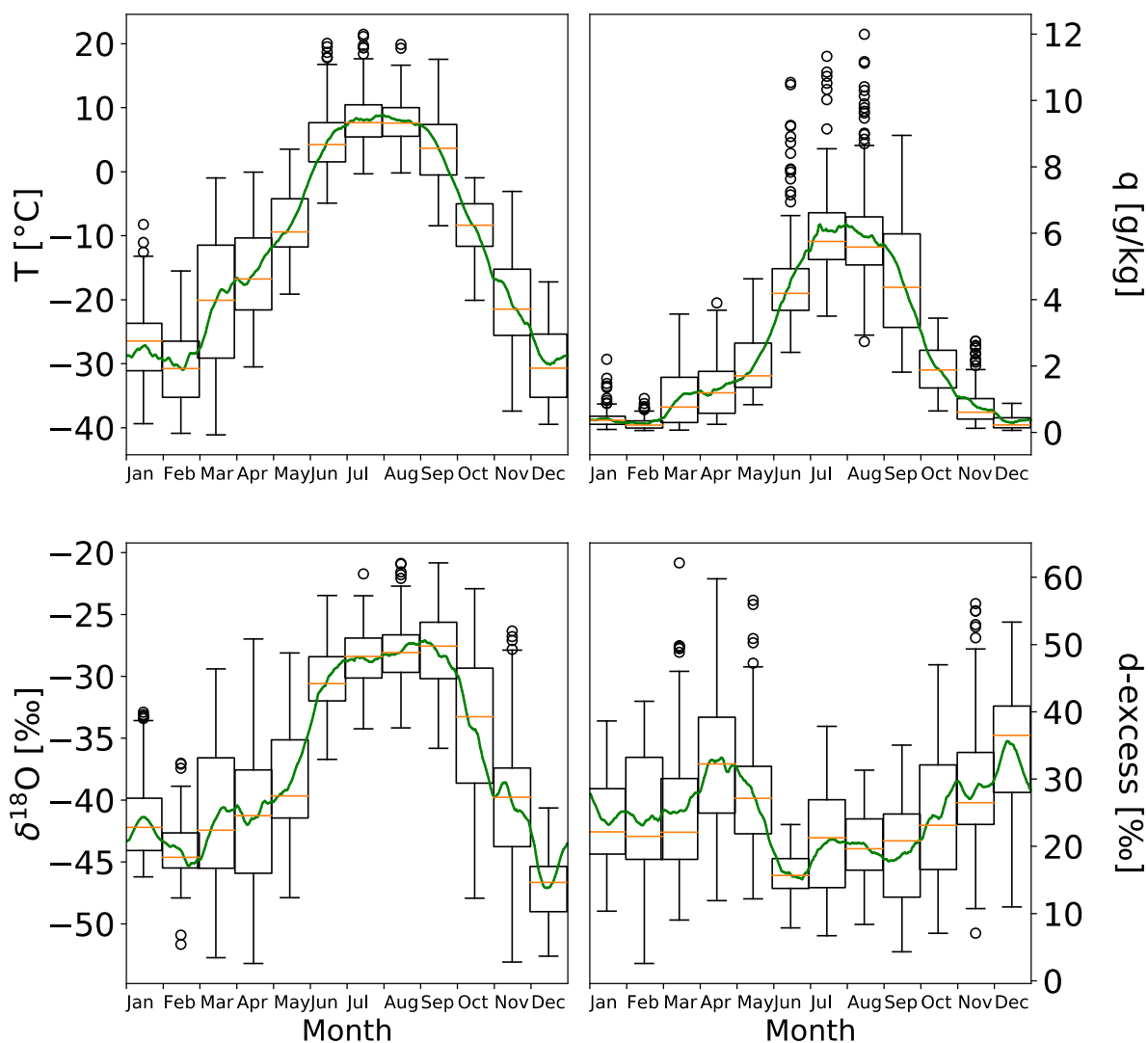
Figure 3: Average seasonal cycle for the period 2015-07-01 to 2017-06-30, for (a) air temperature (°C), (b) specific humidity q (/kg), (c) δ¹⁸Oᵥ (‰) and (d) d-excessᵥ (‰). For boxplots, the boxes represent the first and third quartiles, and the orange bar represents the median; the whiskers represent the lowest (highest) datum still within 1.5 interquartile range (IQR) of the lower (upper) quartile and the outliers are represented as black circles.

3.3 Synoptic variability

The synoptic variations, responsible for variations in the meteorological and water vapour isotopic signals at time scales from a few hours to a few weeks, are related to large-scale meteorological patterns and allow to investigate the influence of remote moisture sources. In order to distinguish these synoptic variations from potential diurnal variations, we use daily averaged values (Supplementary Figure 4). Compared to the seasonal variations, synoptic variations of specific humidity have a large amplitude in summer (on the order of 5 g kg^{-1}) but a low amplitude in winter (on the order of 1 to 2 g kg^{-1}). In contrast, the synoptic variations of air temperature have a large amplitude in winter (up to 20° C) and a lower amplitude in summer (around 10° C). This is coherent with the Clausius-Clapeyron relationship. Frequent episodes of strong relative humidity variations are observed from one day to the next between June and August (variations from down to 60% to up to 100%). During winter, the variations of relative humidity are slow (variations over several weeks) and of lower amplitude (changes in the order of magnitude of 20%) than these fast summer variations.

3.4 Diurnal cycles

We expect diurnal variations of the local evaporation flux to cause diurnal variations of the water vapour isotopic composition. To evaluate the diurnal cycles of meteorological and water isotopic composition, we use datasets averaged at 1-hour temporal resolution. Some periods of relatively stable synoptic situation during spring and summer (wind speed below 5 m.s^{-1} over 24 hours) clearly show significant variations of temperature and relative humidity on the diurnal time scale. We compute the average diurnal cycle of temperature, specific and relative humidity and vapour isotopic composition for these stable synoptic situation periods over different seasons.

No diurnal cycle is seen in any of the parameters for winter and autumn (not presented), which is the period dominated by the polar night. In summer (see Supplementary Figure 3), an average temperature diurnal cycle is found for stable synoptic situation periods with an amplitude of respectively 3°C, which is lower than the typical amplitude of synoptic variations during this season (around 10°C, see Figure 1 and averaged diurnal cycles on Supplementary Figure 3). For these periods of stable synoptic condition, the average diurnal variations of specific humidity is not significant in summer compared to the synoptic variability (the amplitude of the mean cycle is lower than the standard deviation).

The observed summer average diurnal cycle of relative humidity observed (average amplitude of 13.4% average amplitude) is probably due to the diurnal variations of temperature which are not followed by any diurnal variations of the specific humidity. As for the specific humidity signal, there are no significant average diurnal variations of any vapour isotopic signals ($\delta^{18}O_v$, δD_v or d-excess$_v$) for neither season.

During spring, strong changes occur regarding temperature, specific humidity, isotopic composition or insolation within a few weeks. Analyses of the average diurnal cycle for days of stable synoptic situation over a 3 months period from March to May do not reveal any significant diurnal variations of the specific humidity and vapour isotopic composition. However, a comparable analysis over the month of May, only, when the daily variations of the insolation is maximal, reveals significant

average diurnal variations (Figure 4) for temperature (with an amplitude of 4.9°C), relative humidity (amplitude of 5.4%), specific humidity (amplitude of 0.4 g/kg), $\delta^{18}O_v$ (amplitude of 1.1 ‰) and δD_v (amplitude of 10 ‰). The diurnal cycle is not significant for d-excess$_v$, as compared to the observed variability and also smaller than the instrumental precision.

335
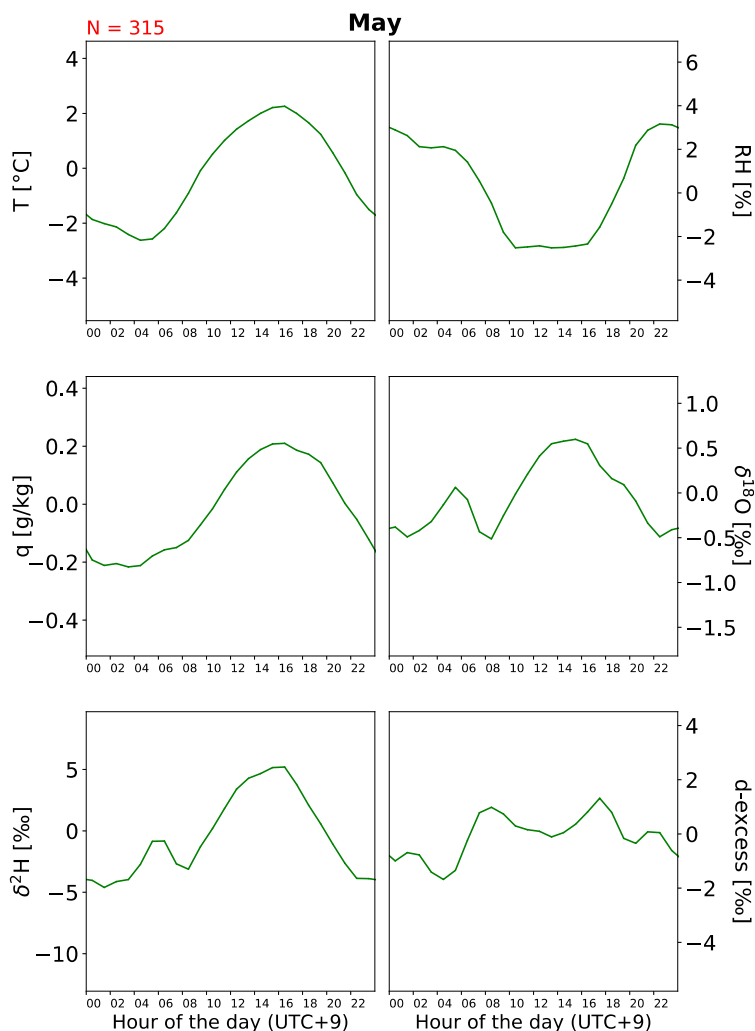
Figure 4: Average daily cycle in May, for the selected days of stable synoptic conditions (wind speed below 5 m.s^{-1} over 24 hours), for T (°C), RH (%), q (g/kg), $\delta^{18}O_v$ (‰), δ^2H_v (‰) and d-excess$_v$ (‰). The daily cycles are calculated with the stacked anomalies compared to the daily average. The local time (UTC+9) is used to present to the results.

340 **4 Discussion**

4.1 Temporal variations of the water isotopic composition

Comparing the precipitation and vapour isotopic composition reveals a large offset between the δ-values, as well as the d-excess values. To investigate the origin of this offset, we calculate a theoretical vapour isotopic composition from the precipitation samples. Important assumptions are made for this calculation: we consider an equilibrium fractionation
345 between vapour and the condensed phase (liquid or solid for positive or negative temperatures) using the temperature measured at 2 m height at the time of the sampling. The calculated theoretical vapour $\delta^{18}O$ and δ^2H ($\delta^{18}O_{v,th}$ and $\delta^2H_{v,th}$) agree with the measured $\delta^{18}O_v$ and δ^2H_v during summer, spring and autumn (Figure 1). The calculated theoretical and measured summer and autumn d-excess values also match, showing that precipitation is in equilibrium with vapour during these seasons (Figure 1). However, large discrepancies remain between the winter and spring calculated theoretical and measured
350 vapour d-excess signals (Figure 1), indicating either that the precipitation formed from a different moisture source than the measured vapour at the surface, and/or that kinetic fractionation occurs during the formation of precipitation during this period, as expected from the theory of snow crystal formation under supersaturation (Jouzel and Merlivat, 1984).

The absence of a significant diurnal cycle in specific humidity and water vapour isotopic composition at our site in summer differs from observations at the more southerly located western Siberia station Kourovka (Bastrikov et al., 2014), where the
355 summer signal is dominated by the diurnal cycle, which has been attributed to a strong contribution of the local evapotranspiration to the moisture budget. The absence of a clear diurnal cycle at the Samoylov site also differs from other high latitude polar locations, like the interior of Greenland and Antarctica, where strong diurnal cycles have been recorded during summer (Casado et al., 2016; Ritter et al., 2016; Steen-Larsen et al., 2014) and attributed to exchange processes between the vapour and the snow-covered surface, which is not the case for our site, where the surrounding area consists of
360 vegetated areas, small lakes and the rivers network of the Lena delta in summer. The diurnal temperature variations at Samoylov are also small compared to observations at Kourovka. Thus, a tentative explanation for the absence of a diurnal cycle of specific humidity and vapour isotopic values at Samoylov might be that the diurnal variations of incoming radiations are insufficient in summer to drive significant variations of the evapotranspiration. However, this explanation is in contradiction to the results of Eddy-covariance observations performed on the Samoylov Island (Helbig et al., 2013), which
365 revealed maxima of evapotranspiration concomitant with peaks of net radiation in June. Another explanation could also be that the isotopic signal of the evaporated flux is too similar to the boundary layer water vapour isotopic signal to cause a significant diurnal isotopic variation even in case of significant evaporation. Altogether, the diurnal cycles of the boundary layer specific humidity and its isotopic composition, which are too small to be identified among the variabilities linked with the synoptic activity, are not the appropriate parameter to evaluate the impact of local evaporation at our site.
370 During spring, a diurnal cycle of the specific humidity and water vapour isotopic composition, as observed in May, could be caused by local moisture exchanges with the surface, as it is the case over the interior of Greenland and Antarctica in

summer (Casado et al., 2016; Ritter et al., 2016; Steen-Larsen et al., 2014) with sublimation of the snow cover when the insolation is high and condensation during the night. Sublimation of the snow cover, still present until end of May and composed of winter precipitation with $\delta^{18}O_v$ values situated between -20 and -30 ‰, would create moisture with $\delta^{18}O_v$ values

375   higher than the boundary layer water vapour (mean monthly $\delta^{18}O_v$ of -38.6 ‰).

Concerning the seasonal variations of the water vapour isotopic composition, the $\delta^{18}O_v$ values are primarily driven by the variations of temperature and humidity, following the principles of Rayleigh distillation. A possible explanation of the enriched values of $\delta^{18}O_v$ observed at temperatures below -20 °C is that the contribution of local moisture sources is strongly impacting on $\delta^{18}O_v$ signals in an already very dry air.

380   The late-autumn/early winter maximum of d-excess$_v$ observed at Samoylov is similar to water isotopic measurements from precipitation samples along the Lena river in Zhigansk (66.8°N, 123.4°E, 92 m above sea level, approximately 635 km south from Samoylov station) depicting a maximum of d-excess$_v$ from October to December (Kurita, 2011). This peak of d-excess$_v$ has been interpreted as a signal linked with the sea-ice growth in the Arctic Ocean and fast oceanic evaporation occurring at low relative humidity during this period. Maxima of d-excess$_v$ in late-autumn have also been observed in different locations,

385   in particular around the North-Atlantic sector (Bonne et al., 2014; Steen-Larsen et al., 2015). The very low relative humidity values above the ocean where the evaporation takes place in this season could explain these high d-excess$_v$ values (Pfahl and Sodemann, 2014; Steen-Larsen et al., 2014). The other spike of d-excess$_v$ observed in April/May is not concomitant with low relative humidity. It might however be an indicator of sublimation processes taking place. During this period, temperatures are still low but rapidly rising (monthly average temperatures of -8.4°C in May), snow cover is decreasing and the solar

390   radiation increases with important diurnal variations. The interpretation of this high d-excess$_v$ period as an effect of sublimation agrees with our explanation of the diurnal cycle observed in May.

4.2 Moisture sources variations at the seasonal scale

Changes of the moisture sources can affect water stable isotopic composition. Firstly, due to the link between temperature difference and spatial transport: the longer the moisture has been transported from the evaporation source, the more

395   distillation an air mass might have undergone on the way. Secondly, the meteorological conditions at which the evaporation takes place will influence the isotopic composition of the initial vapour. Finally, different (primary and secondary) evaporation sources can have different isotopic signals. We focus here on the seasonal changes of the moisture sources from the averaged outputs of the semi-Lagrangian backward trajectories simulation and moisture source diagnostics over different seasons (Figures 5, 6).

400   The overall amount of evaporation is strongly season-dependent (Figure 5), which reflects in the seasonality of the specific humidity measured at our site. During the winter months (December, January, February; DJF), the area with the highest moisture uptakes is situated above the Barents and Norwegian Seas (Figure 5.a). The moisture origin is therefore particularly distant from our site and long-distance transport dominates over local processes. For spring (March, April, May; MAM) and

autumn (September, October, November; SON), an enhanced continental evaporation is observed over a large part of

405   Siberia, contrary to winter. The main moisture uptake is located along the northern part of the Lena river basin. Minor oceanic sources are also revealed in some areas of the Arctic Ocean (*Figure 5*.d). In spring, only parts of the Barents and Norwegian Seas depict moisture uptake, while it is also the case for the Laptev, Kara and East Siberian Seas in autumn (Figure 5.b), which is coherent with the sea ice covering these last regions in spring, preventing oceanic evaporation, but not during the first autumn months. In summer (June, July, August; JJA), more air masses originate from the western Arctic

410   Ocean than in winter. Despite the large ice-free surface in the Arctic during summer, the moisture uptake remains very low over the Arctic Ocean compared to the evapotranspiration taking place locally over the continent (Figure 5.c). The most predominant moisture uptake occurs locally above continental areas, mainly southwest of our site (Figure 5.c). Local vegetation, lakes, ponds and rivers are the potential sources of evapotranspiration which can generate such regional moisture uptake in summer (due to the absence of snow and ice covers in this season).

415   For all seasons, the average difference between evaporation and precipitation shows a general pattern of dominant precipitation at high latitudes and dominant evaporation at low latitudes (Figure 6). The limit at which the precipitation prevails over evaporation is different for continental and oceanic regions. It is relatively stable around 50°N above the ocean, but its latitude varies from 60°N in summer and 45°N in winter over the continent (Figure 6). At our site, precipitation is always predominant over evaporation at any season.

420   The local moisture uptake in the region surrounding the station in particular in summer can, however, contribute to the water vapour isotopic signal, even if evaporation is lower than precipitation. Local evapotranspiration sources exist in summer, such as the vegetation, ponds and lakes and the Lena river. As these sources are not active during the cold seasons, sublimation of the snow cover can act as a local moisture source, as previously suggested from the diurnal cycle revealed in spring.
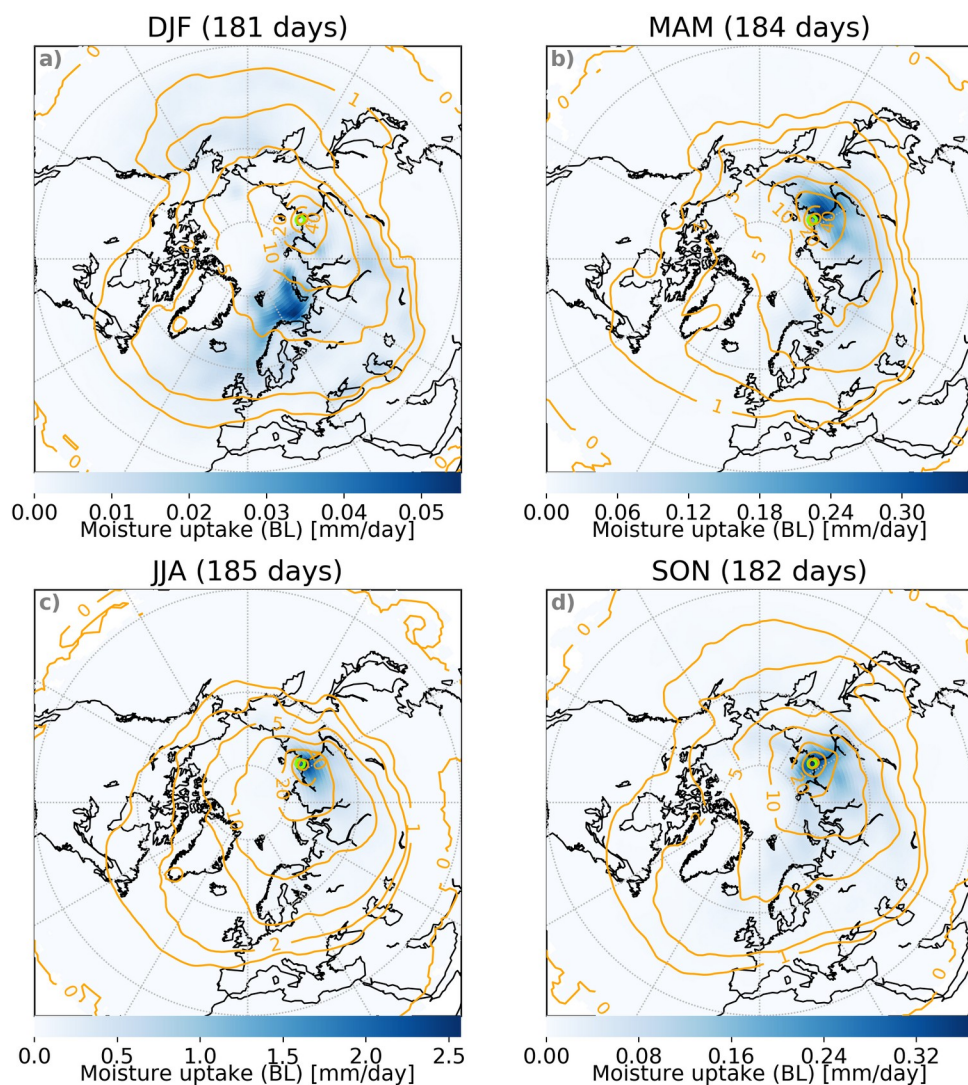
425

Figure 5: Seasonal averages of boundary layer moisture uptake in mm/day for the period 2015-07-01 to 2017-07-01. For (a) winter, (b) spring, (c) summer and (d) autumn periods. The orange contour lines indicate the trajectories locations (as percentage of maximum value: 80, 40, 20, 10, 5, 2, 1 and 0%). The green circles indicate the location of the Samoylov station.
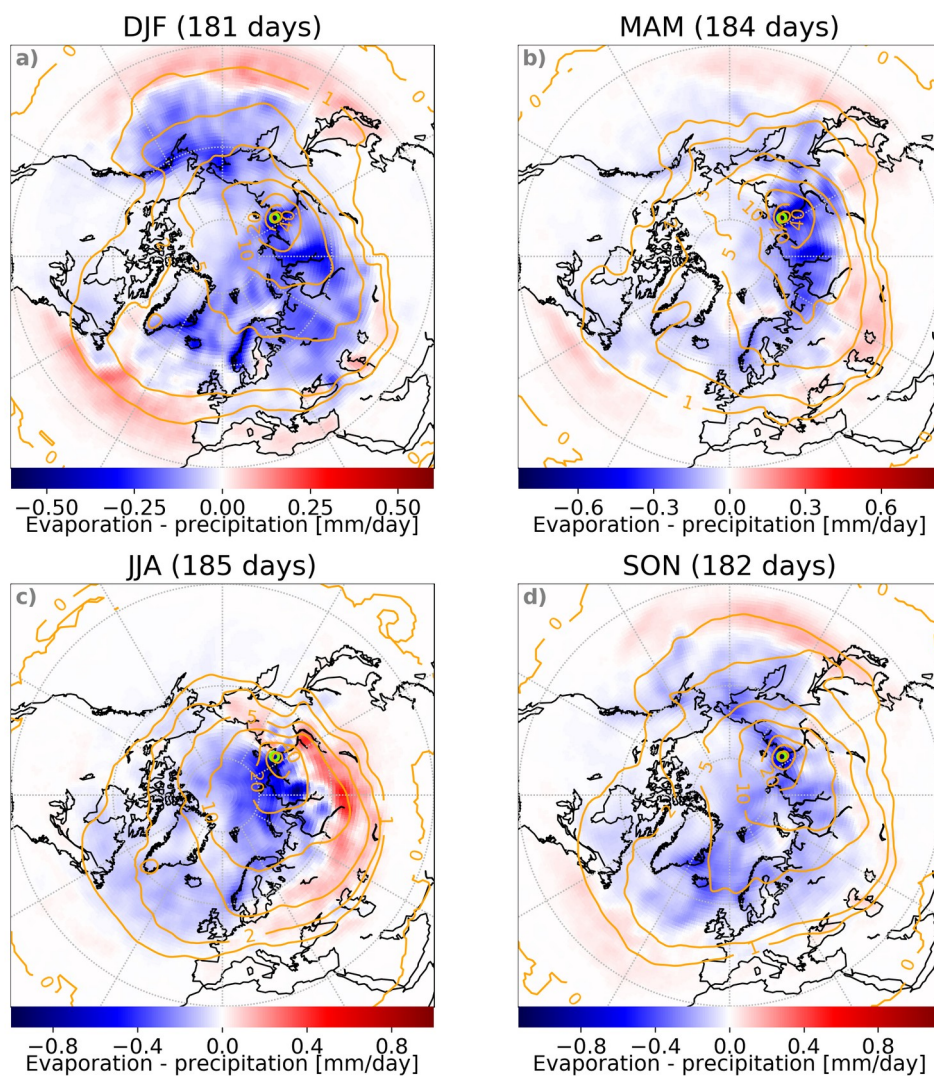
430

Figure 6: Same as Figure 5, with colours indicating the seasonal averages of evaporation minus precipitation (in mm/day): red (blue) colours indicate regions where evaporation is stronger (respectively weaker) than precipitation.

4.3 Seasonal versus synoptic variabilities and water vapour isotopic composition

4.3.1 Influence of the wind origin

To evaluate the impact of these seasonal moisture origin changes on the water vapour isotopic composition, we focus in this section on the statistical distribution of specific humidity and isotopes as a function of the wind direction observed at our site (Figure 7).

The summer season (JJA) presents a relatively homogeneous wind distribution: winds from all sectors represent between 4.3 and 8.6% of the observations (Figure 7). No wind sector is exclusively associated to a single range of specific humidity or water vapour isotopic values, but the frequencies of occurrences for these values still vary with the wind direction. However, the highest values of specific humidity originate from the south-south-east, thus along the Lena river basin (Figure 7.a). The most enriched $\delta^{18}O_v$ values and the lowest d-excess$_v$ values derive from a wide range of western sectors, while a higher proportion of depleted $\delta^{18}O_v$ values and the highest d-excess$_v$ values are associated with air masses originating from the east (Figure 7.b,c). This provides a potential way to differentiate between the moisture sources originating from the Atlantic and the Pacific sectors.

We investigate the coldest months, from December to April (DJFAM), as they are the relevant months to contribute to the interpretation of the paleoclimate data retrieved from ice wedges in our research area. Contrary to the summer period, the cold months wind distribution exhibits a strongly predominant situation, with most winds originating from the south-south-east (20.6%) and the south sectors (16.3%) i.e. along the orographic barrier of the Verkhoyansk mountains. As for the summer season, all wind sectors present similar ranges of specific humidity and water vapour isotopic composition, but with different distributions. The south and south-south-east sectors are associated with a stronger proportion of very dry air (between 0.1 and 0.6 g/kg, Figure 7.d), and of the isotopically most depleted vapour ($\delta^{18}O_v$ below -45.7‰, Figure 6.e), compared to the other sectors. These very low $\delta^{18}O_v$ values associated with air masses originating from the continent are consistent with the absence of moisture uptakes above a large part of the continent during this period (Figure 6). These air masses therefore undergo a strong isotopic distillation above the continent before reaching our site. For the air masses originating from the south-west, north-west or north-east, some significantly closer moisture sources can contribute to the isotopic composition of air masses (significant moisture uptakes exist in the north Atlantic and North Pacific sectors, as depicted on Figure 6). This is reflected in a higher proportion of high $\delta^{18}O_v$ values for these wind sectors, compared to the air masses originating from the south and south-south-east sectors. The most enriched air masses ($\delta^{18}O_v$ above -30.7‰) originate from the North-West sector (Figure 7.e).
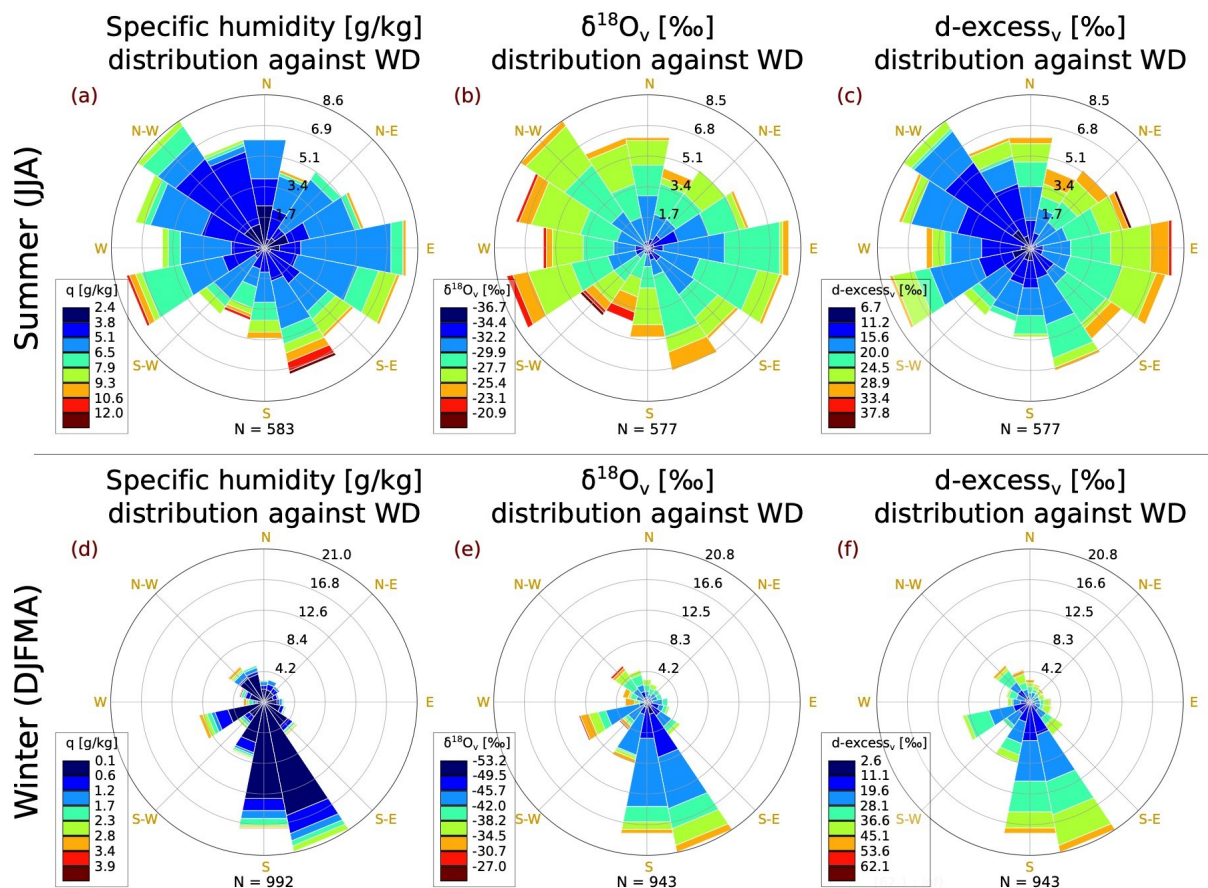
Figure 7: Percent distribution of (a,d) specific humidity, (b,e) $\delta^{18}O_v$ and (c,f) d-excess$_v$: for (a, b, c) the summer months only (June to August) and (d, e, f) the cold months only (from December to April).The percent distributions are given with respect to the different wind directions (WD).

4.3.2 Influence of the moisture source

As previously described, notable differences of water vapour isotopic composition exist between wind sectors during the winter season, in particular for the extreme high and low $\delta^{18}O_v$ values. As the local wind direction only provides information on the final step of air masses transport, we further investigate the outputs of the moisture sources diagnostics associated with synoptic events of extreme isotopic values.

For the coldest months (December to April), a selection of extreme values based on the distance to a 60-days running average for temperature, the logarithm of specific humidity, $\delta^{18}O_v$ and d-excess$_v$ shows strong similarities for the different parameters considered (Figure 8 and Supplementary Tables 1 and 2). Many synoptic events of short duration occurring on a daily time-scale, are selected independently for the different parameters. However, some patterns emerge with periods of several weeks where extrema are identified on multiple parameters, even if the extrema are not always happening at the

exact same date for all parameters. Two typical situations are predominant: on one side, a typical pattern of high temperature, specific humidity and $\delta^{18}O_v$ but low d-excess$_v$; on the other side, an opposite pattern characterised by low

480   temperature, specific humidity and $\delta^{18}O_v$ but high d-excess$_v$. Since the long-lasting events dominate this selection and are usually selected for all parameters, the associated average moisture source diagnostics are very similar for all parameters (Figure 9).

The first transport pattern (Figure 9.b,d,f,h), characterized by high temperature, specific humidity and $\delta^{18}O_v$ but low d-excess$_v$, is associated with long-range transport of air masses originating from the west. Air masses originate from North-

485   western Eurasia, up to the Lena river on the eastern limit, and from the southwestern Arctic Ocean. Precipitation is stronger than evaporation above the northernmost sectors of western Eurasia and over a large part of the Arctic Ocean. However, evaporation is stronger than precipitation over the northern European seas (North, Norwegian, Barents and Baltic Seas) and for continental areas located up to 60°N. The fast transport of air masses with only moderate precipitation brings moisture from the sources to our site with relatively high $\delta^{18}O_v$ values for this season.

490   The second pattern (Figure 9.a,c,e,g), characterised by low temperature, specific humidity and $\delta^{18}O_v$ but high d-excess$_v$, is associated with more local air masses, predominantly originating from the east. Precipitation is stronger than evaporation over whole Northern Eurasia as well as all polar and sub-polar Oceans. Evaporation is only dominant in very remote locations, like the subtropical North Pacific Ocean and the mid-latitudinal Atlantic Ocean. The moisture sources are therefore much more distant for this pattern than for the opposite pattern and the isotopic distillation can be much stronger,

495   therefore the $\delta^{18}O_v$ values associated to these atmospheric transport patterns are lower.

The first pattern of high temperature in winter previously described presents some similarities with the average summer situation, such as a predominance of air masses originating from the west. If the limit of net evaporation compared to precipitation is situated at higher latitudes for the high temperatures pattern than for the low temperatures pattern, there are still fewer net sources of evaporation over the continent than in summer.
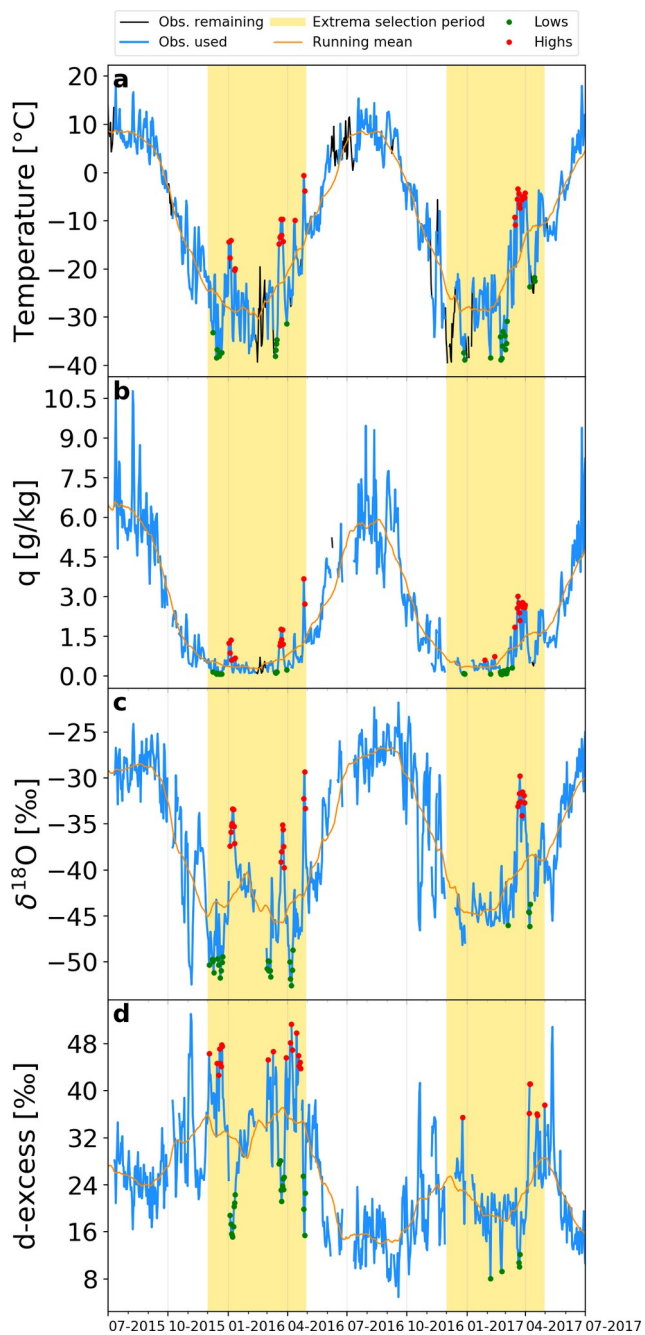
Figure 8: Time series of (a) temperature, (d) specific humidity, (g) δ^{18}O$_v$ and (j) d-excess$_v$. The daily averaged data are depicted in blue for the data used to compute the 60-days running average (orange line) and in black for the remaining data (not used in the running average calculation). The selected high and low extrema are respectively shown as red and green dots. The yellow shade represents the period over which the extrema are considered: from December to April for each year.
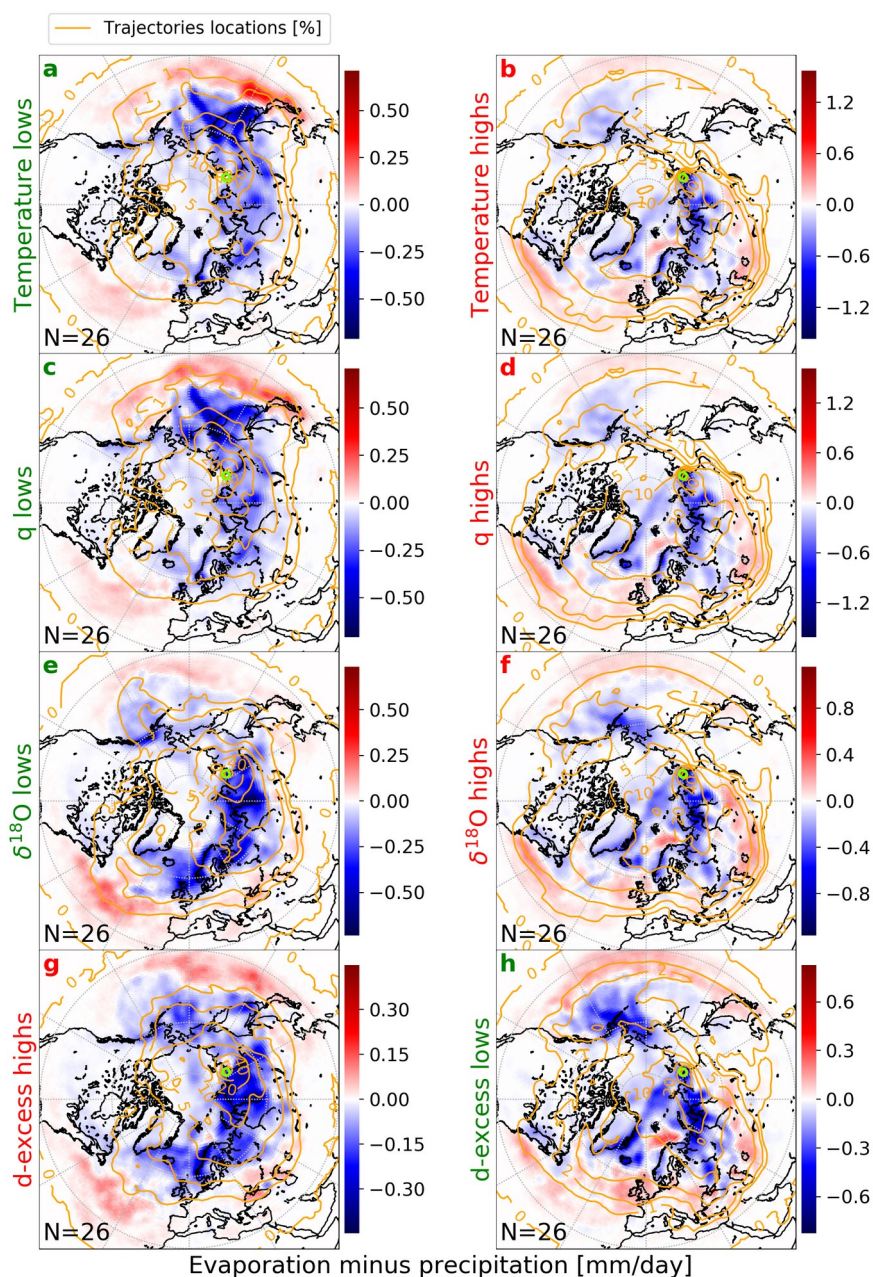
Figure 9: Average "evaporation minus precipitation" for the selection of low and high extrema over the December to April period, as depicted on Figure 8: for temperature lows (a) and highs (b), for specific humidity lows (c) and highs (d), for $\delta^{18}O_v$ lows (e) and highs (f) and for d-excess$_v$ highs (g) and lows (h). The orange contour lines indicate the trajectories locations (as percentage of maximum value: 80, 40, 20, 10, 5, 2, 1 and 0%). The green circles indicate the location of the Samoylov station.

5 Conclusions

This study presents two years of *in situ* continuous water vapour isotopic observations in the Siberian Arctic on the
515   Samoylov Island in the Lena river delta, starting in July 2015.

This new dataset provides information about the moisture isotopic composition which are complementary to the precipitation samples isotopic composition, as they also provide information for dry periods when no precipitation falls. It also allows comparing the water isotopic composition in both phases and distinguish periods when precipitation and vapour are at equilibrium (in summer and autumn) or out of equilibrium (during winter and spring). This comparison therefore highlights
520   the kinetic fractionation processes occurring during the formation of snow in the cold periods.

The water vapour isotope dynamics is dominated by seasonal and synoptic variations. During the coldest months, the observed humidity and water vapour isotopic composition are comparable to summer observations on the East Antarctic plateau. The diversity of isotopic signals associated with long-range transported moisture from various remote origins has a strong imprint on the vapour isotopic composition observed at the Samoylov station.

525   In summer, the observed diurnal cycle of temperature has a low amplitude and is not clearly mirrored by diurnal cycles of the specific humidity and vapour isotopic compositions, but overwhelmed by variations linked to synoptic activity. Our data indicate either that the local sources of humidity are not strongly varying at a diurnal scale or that the isotopic signal of a local source is not distinguishable from the remotely transported moisture in this season. The situation is different during spring, when the insolation is strongly varying between day and night and the surface is still covered by snow. During this
530   period, significant diurnal variations of the specific humidity and water vapour isotopic composition are revealed, which indicates moisture exchange processes between the boundary layer atmosphere and the surface, with a potential influence of snow cover sublimation. It is however difficult to independently evaluate the imprints on the vapour isotopic composition of each potential individual local moisture source (vegetated or snow-covered land, open or frozen river, open over sea ice covered Laptev sea), as many changes of the surface cover happen simultaneously within a few weeks at this period, as well
535   as in autumn, and may affect the local hydrological cycle.

Evaluations of the moisture sources, based on semi-Lagrangian backtrajectories simulations, show small but significant changes of air masses origin at the seasonal scale. Depending on the seasons, areas of air masses origins differently contribute to the moisture balance of our study area. In the region surrounding Samoylov station, significant moisture uptake from the surface is found in summer and to a lower extent in spring and autumn, which contributes to the observed vapour
540   isotopic signal, while such local surface moisture uptake is almost inexistent in winter. Despite the local surface moisture uptake, the precipitation predominates over surface moisture uptakes on average for all seasons over the region surrounding our site. Surface moisture uptakes are predominant over precipitation for some remote locations only, over the Atlantic and Pacific Oceans as well as over the Eurasian continent, south of a limit which moves southwards during the cold seasons and northward during the warm seasons. The main moisture sources are therefore generally more distant from our research area
545   in winter than in summer.

On the synoptic time scale, it is not possible to exclusively attribute all observed vapour isotopic signals to a specific moisture source. However, there are statistical differences in the vapour vapour isotopic distribution related with the moisture origin which provides a potential way to identify moisture source changes from recorded isotopic compositions. In summer, the most enriched $\delta^{18}O_v$ values and the lowest d-excess$_v$ values are associated with air masses originating from the west (Atlantic sector), while a higher proportion of depleted $\delta^{18}O_v$ values and the highest d-excess$_v$ values are associated with air masses originating from the east (Pacific sector). During the cold months (December to April), cold and dry air with isotopically depleted vapour and high d-excess$_v$ is associated with stagnant air masses above northern Eurasia, and vapour originating either from the Pacific (the most common situation) or from the Atlantic sectors. The significant contribution of eastbound moisture source from the Pacific regions is a new finding of this study. During the same period, an opposite situation of warm, moist air with isotopically enriched vapour and low values of d-excess$_v$ is typically associated with air masses originating from the North-Atlantic basin and transported via westerlies rapidly towards our site. Such events are frequently observed between March and mid-April, associated with an early spring increase of temperature, humidity and $\delta^{18}O_v$.

Our study contributes to an improved knowledge of the variations of water isotopic composition from the seasonal to the synoptic scale in the eastern Arctic continental region. It will help improving the interpretation of water isotopes paleoclimate proxies based on ice wedges retrieved in the region (e.g., Meyer et al., 2015). It contributes to the understanding of the moisture sources and atmospheric transport processes. It is also a baseline for studies of future changes in the region, as many hydrological changes are expected in the region, in particular with retreating sea ice over the Arctic Ocean, which might trigger more effective contributions from this moisture source and affect the water isotopic composition in vapour and precipitation.

Appendices

Supplementary information is available in the online version of the paper.

Reprints and permissions information is available online at www.nature.com/reprints. Correspondence and requests for materials should be addressed to J.-L.B or M.W.

Data availability

All presented instrumental and modelling data of this study are available on the PANGAEA database with instructions about data format and necessary treatments.

Author contributions

All authors contributed to the design of this study. Instrument layout and Picarro installation on Samoylov was done by J.-575 L.B., M.B., H.M., S.K., L.S., H.C.S.-L., and M.W. Isotope measurements and instrument maintenance were performed by J.-L.B., H.M. and M.W. The first manuscript draft was written by J.-L.B. and M.W., and all authors contributed to the discussion of results and the final article.

Acknowledgements

This study has been funded by the AWI strategy fund project ISOARC.
580 We acknowledge the AARI, AWI and MPI SB RAS logistics for the invaluable support of the Russian-German LENA Expeditions and the Research Station Samoylov Island of IPGG SB RAS and its staff for support of our field work, in particular Andrei Astapov for help with the daily maintenance of the laser spectrometer.
We acknowledge the use of imagery from the NASA Worldview application (https://worldview.earthdata.nasa.gov), part of the NASA Earth Observing System Data and Information System (EOSDIS).

585 **References**

Bailey, A., Noone, D., Berkelhammer, M., Steen-Larsen, H. C. and Sato, P.: The stability and calibration of water vapor isotope ratio measurements during long-term deployments, Atmos. Meas. Tech., 8(10), 4521–4538, doi:10.5194/amt-8-4521-2015, 2015.

Bastrikov, V., Steen-Larsen, H. C., Masson-Delmotte, V., Gribanov, K., Cattani, O., Jouzel, J. and Zakharov, V.: Continuous measurements of atmospheric water vapour isotopes in Western Siberia (Kourovka), Atmos. Meas. Tech. Discuss., 7(1), 475–507, doi:10.5194/amtd-7-475-2014, 2014.

Benetti, M., Reverdin, G., Pierre, C., Merlivat, L., Risi, C., Steen-Larsen, H. C. and Vimeux, F.: Deuterium excess in marine water vapor: dependency on relative humidity and surface wind speed during evaporation, Journal of Geophysical Research: Atmospheres, 119, 584–593, doi:10.1002/2013JD020535, 2014.

Benetti, M., Steen-Larsen, H. C., Reverdin, G., Sveinbjörnsdottir, A. E., Aloisi, G., Berkelhammer, M. B., Bourlès, B., Bourras, D., Coetlogon, G. de, Cosgrove, A., Faber, A.-K., Grelet, J., Hansen, S. B., Johnson, R., Legoff, H., Martin, N., Peters, A. J., Popp, T. J., Reynaud, T. and Winther, M.: Stable isotopes in the atmospheric marine boundary layer water vapour over the Atlantic Ocean, 2012–2015, Scientific Data, 4, 160128, doi:10.1038/sdata.2016.128, 2017.

Biskaborn, B. K., Smith, S. L., Noetzli, J., Matthes, H., Vieira, G., Streletskiy, D. A., Schoeneich, P., Romanovsky, V. E., Lewkowicz, A. G., Abramov, A., Allard, M., Boike, J., Cable, W. L., Christiansen, H. H., Delaloye, R., Diekmann, B., Drozdov, D., Etzelmüller, B., Grosse, G., Guglielmin, M., Ingeman-Nielsen, T., Isaksen, K., Ishikawa, M., Johansson, M., Johannsson, H., Joo, A., Kaverin, D., Kholodov, A., Konstantinov, P., Kröger, T., Lambiel, C., Lanckman, J.-P., Luo, D., Malkova, G., Meiklejohn, I., Moskalenko, N., Oliva, M., Phillips, M., Ramos, M., Sannel, A. B. K., Sergeev, D., Seybold,

C., Skryabin, P., Vasiliev, A., Wu, Q., Yoshikawa, K., Zheleznyak, M. and Lantuit, H.: Permafrost is warming at a global scale, Nature Communications, 10(1), 264, doi:10.1038/s41467-018-08240-4, 2019.

Boike, J., Kattenstroth, B., Abramova, E., Bornemann, N., Chetverova, A., Fedorova, I., Fröb, K., Grigoriev, M., Grüber, M., Kutzbach, L., Langer, M., Minke, M., Muster, S., Piel, K., Pfeiffer, E.-M., Stoof, G., Westermann, S., Wischnewski, K., Wille, C. and Hubberten, H.-W.: Baseline characteristics of climate, permafrost and land cover from a new permafrost observatory in the Lena River Delta, Siberia (1998-2011), Biogeosciences (BG), 10, 2105–2128, doi:10.5194/bg-10-2105-2013, 2013.

Boike, J., Nitzbon, J., Anders, K., Grigoriev, M., Bolshiyanov, D., Langer, M., Lange, S., Bornemann, N., Morgenstern, A., Schreiber, P., Wille, C., Chadburn, S., Gouttevin, I., Burke, E. and Kutzbach, L.: A 16-year record (2002–2017) of permafrost, active-layer, and meteorological conditions at the Samoylov Island Arctic permafrost research site, Lena River delta, northern Siberia: an opportunity to validate remote-sensing data and land surface, snow, and permafrost models, Earth System Science Data, 11(1), 261–299, doi:https://doi.org/10.5194/essd-11-261-2019, 2019a.

Boike, J., Nitzbon, J., Anders, K., Grigoriev, M. N., Bolshiyanov, D. Y., Langer, M., Lange, S., Bornemann, N., Morgenstern, A., Schreiber, P., Wille, C., Chadburn, S., Gouttevin, I. and Kutzbach, L.: Measurements in soil and air at Samoylov Station (2002-2018), version 201908, Alfred Wegener Institute - Research Unit Potsdam [online] Available from: https://doi.pangaea.de/10.1594/PANGAEA.905236 (Accessed 16 September 2019b), 2019.

Bonne, J.-L., Masson-Delmotte, V., Cattani, O., Delmotte, M., Risi, C., Sodemann, H. and Steen-Larsen, H. C.: The isotopic composition of water vapour and precipitation in Ivittuut, southern Greenland, Atmos. Chem. Phys., 14(9), 4419–4439, doi:10.5194/acp-14-4419-2014, 2014.

Bonne, J.-L., Steen-Larsen, H. C., Risi, C., Werner, M., Sodemann, H., Lacour, J.-L., Fettweis, X., Cesana, G., Delmotte, M., Cattani, O., Vallelonga, P., Kjær, H. A., Clerbaux, C., Sveinbjörnsdóttir, A. E. and Masson-Delmotte, V.: The summer 2012 Greenland heat wave: In situ and remote sensing observations of water vapor isotopic composition during an atmospheric river event, J. Geophys. Res. Atmos., 120(7), 2014JD022602, doi:10.1002/2014JD022602, 2015.

Bonne, J.-L., Behrens, M., Meyer, H., Kipfstuhl, S., Rabe, B., Schönicke, L., Steen-Larsen, H. C. and Werner, M.: Resolving the controls of water vapour isotopes in the Atlantic sector, Nature Communications, 10(1), 1632, doi:10.1038/s41467-019-09242-6, 2019.

Butzin, M., Werner, M., Masson-Delmotte, V., Risi, C., Frankenberg, C., Gribanov, K., Jouzel, J. and Zakharov, V. I.: Variations of oxygen-18 in West Siberian precipitation during the last 50 years, Atmos. Chem. Phys., 14(11), 5853–5869, doi:10.5194/acp-14-5853-2014, 2014.

Casado, M., Landais, A., Masson-Delmotte, V., Genthon, C., Kerstel, E., Kassi, S., Arnaud, L., Picard, G., Prie, F., Cattani, O., Steen-Larsen, H.-C., Vignon, E. and Cermak, P.: Continuous measurements of isotopic composition of water vapour on the East Antarctic Plateau, Atmospheric Chemistry and Physics Discussions, 1–26, doi:10.5194/acp-2016-8, 2016.

Coplen, T. B.: Guidelines and recommended terms for expression of stable-isotope-ratio and gas-ratio measurement results, Rapid Communications in Mass Spectrometry, 25(17), 2538–2560, doi:10.1002/rcm.5129, 2011.

Craig, H.: Isotopic variations in meteoric waters, Science, 133(3465), 1702–1703, doi:10.1126/science.133.3465.1702, 1961.

Dansgaard, W.: Stable isotopes in precipitation, Tellus, 16(4), 436–468, doi:10.1111/j.2153-3490.1964.tb00181.x, 1964.

Dee, D. P., Uppala, S. M., Simmons, A. J., Berrisford, P., Poli, P., Kobayashi, S., Andrae, U., Balmaseda, M. A., Balsamo, G., Bauer, P., Bechtold, P., Beljaars, A. C. M., van de Berg, L., Bidlot, J., Bormann, N., Delsol, C., Dragani, R., Fuentes, M., Geer, A. J., Haimberger, L., Healy, S. B., Hersbach, H., Hólm, E. V., Isaksen, L., Kållberg, P., Köhler, M., Matricardi, M., McNally, A. P., Monge-Sanz, B. M., Morcrette, J.-J., Park, B.-K., Peubey, C., de Rosnay, P., Tavolato, C., Thépaut, J.-N. and Vitart, F.: The ERA-Interim reanalysis: configuration and performance of the data assimilation system, Q.J.R. Meteorol. Soc., 137(656), 553–597, doi:10.1002/qj.828, 2011.

Dütsch, M., Pfahl, S., Meyer, M. and Wernli, H.: Lagrangian process attribution of isotopic variations in near-surface water vapour in a 30-year regional climate simulation over Europe, Atmos. Chem. Phys. Discuss., 2017, 1–26, doi:10.5194/acp-2017-744, 2017.

Galewsky, J., Steen-Larsen, H. C., Field, R. D., Worden, J., Risi, C. and Schneider, M.: Stable isotopes in atmospheric water vapor and applications to the hydrologic cycle, Reviews of Geophysics, 54(4), 809–865, doi:10.1002/2015RG000512, 2016.

Gribanov, K., Jouzel, J., Bastrikov, V., Bonne, J.-L., Breon, F.-M., Butzin, M., Cattani, O., Masson-Delmotte, V., Rokotyan, N., Werner, M. and Zakharov, V.: Developing a western Siberia reference site for tropospheric water vapour isotopologue observations obtained by different techniques (in situ and remote sensing), Atmos. Chem. Phys., 14(12), 5943–5957, doi:10.5194/acp-14-5943-2014, 2014.

Grigoriev, N. F.: The temperature of permafrost in the Lena delta basin–deposit conditions and properties of the permafrost in Yakutia, Yakutsk, 2, 97–101, 1960.

Guilpart, E., Vimeux, F., Evan, S., Brioude, J., Metzger, J.-M., Barthe, C., Risi, C. and Cattani, O.: The isotopic composition of near-surface water vapor at the Maïdo observatory (Reunion Island, southwestern Indian Ocean) documents the controls of the humidity of the subtropical troposphere, Journal of Geophysical Research: Atmospheres, 122(18), 9628–9650, doi:10.1002/2017JD026791, 2017.

Helbig, M., Boike, J., Langer, M., Schreiber, P., Runkle, B. R. K. and Kutzbach, L.: Spatial and seasonal variability of polygonal tundra water balance: Lena River Delta, northern Siberia (Russia), Hydrogeol J, 21(1), 133–147, doi:10.1007/s10040-012-0933-4, 2013.

Jouzel, J. and Merlivat, L.: Deuterium and oxygen 18 in precipitation: Modeling of the isotopic effects during snow formation, Journal of Geophysical Research: Atmospheres, 89(D7), 11749–11757, doi:10.1029/JD089iD07p11749, 1984.

Kopec, B. G., Lauder, A. M., Posmentier, E. S. and Feng, X.: The diel cycle of water vapor in west Greenland, J. Geophys. Res. Atmos., 119(15), 2014JD021859, doi:10.1002/2014JD021859, 2014.

Kurita, N.: Origin of Arctic water vapor during the ice-growth season, Geophysical Research Letters, 38(2), doi:10.1029/2010GL046064, 2011.

Madsen, M. V., Steen-Larsen, H. C., Hörhold, M., Box, J., Berben, S. M. P., Capron, E., Faber, A.-K., Hubbard, A., Jensen, M. F., Jones, T. R., Kipfstuhl, S., Koldtoft, I., Pillar, H. R., Vaughn, B. H., Vladimirova, D. and Dahl-Jensen, D.: Evidence of Isotopic Fractionation During Vapor Exchange Between the Atmosphere and the Snow Surface in Greenland, Journal of Geophysical Research: Atmospheres, 0(0), doi:10.1029/2018JD029619, 2019.

Majoube, M.: Fractionnement en oxygène 18 entre la glace et la vapeur d'eau, J. Chem. Phys, 68, 625–636, 1971a.

Majoube, M.: Fractionnement en oxygène 18 et en deutérium entre l'eau et sa vapeur, J. Chim. phys, 68(10), 1423–1436, 1971b.

Merlivat, L. and Jouzel, J.: Global climatic interpretation of the deuterium-oxygen 18 relationship for precipitation, Journal of Geophysical Research: Oceans, 84(C8), 5029–5033, doi:10.1029/JC084iC08p05029, 1979.

Merlivat, L. and Nief, G.: Fractionnement isotopique lors des changements d'état solide-vapeur et liquide-vapeur de l'eau à des températures inférieures à 0 degré C, Tellus, 19(1), 122–127, doi:10.1111/j.2153-3490.1967.tb01465.x, 1967.

Meyer, H., Schönicke, L., Wand, U., Hubberten, H. W. and Friedrichsen, H.: Isotope Studies of Hydrogen and Oxygen in Ground Ice - Experiences with the Equilibration Technique, Isotopes in Environmental and Health Studies, 36(2), 133–149, doi:10.1080/10256010008032939, 2000.

Meyer, H., Opel, T., Laepple, T., Dereviagin, A. Y., Hoffmann, K. and Werner, M.: Long-term winter warming trend in the Siberian Arctic during the mid- to late Holocene, Nature Geosci, 8(2), 122–125, doi:10.1038/ngeo2349, 2015.

Pang, H., Hou, S., Landais, A., Masson-Delmotte, V., Jouzel, J., Steen-Larsen, H. C., Risi, C., Zhang, W., Wu, S., Li, Y., An, C., Wang, Y., Prie, F., Minster, B., Falourd, S., Stenni, B., Scarchilli, C., Fujita, K. and Grigioni, P.: Influence of Summer Sublimation on δD, δ18O, and δ17O in Precipitation, East Antarctica, and Implications for Climate Reconstruction From Ice Cores, Journal of Geophysical Research: Atmospheres, 124(13), 7339–7358, doi:10.1029/2018JD030218, 2019.

Pfahl, S. and Sodemann, H.: What controls deuterium excess in global precipitation?, Clim. Past, 10(2), 771–781, doi:10.5194/cp-10-771-2014, 2014.

Ritter, F., Steen-Larsen, H. C., Werner, M., Masson-Delmotte, V., Orsi, A., Behrens, M., Birnbaum, G., Freitag, J., Risi, C. and Kipfstuhl, S.: Isotopic exchange on the diurnal scale between near-surface snow and lower atmospheric water vapor at Kohnen station, East Antarctica, The Cryosphere, 10(4), 1647–1663, doi:https://doi.org/10.5194/tc-10-1647-2016, 2016.

Sodemann, H., Schwierz, C. and Wernli, H.: Interannual variability of Greenland winter precipitation sources: Lagrangian moisture diagnostic and North Atlantic Oscillation influence, Journal of Geophysical Research: Atmospheres, 113(D3), doi:10.1029/2007JD008503, 2008.

Steen-Larsen, H. C., Johnsen, S. J., Masson-Delmotte, V., Stenni, B., Risi, C., Sodemann, H., Balslev-Clausen, D., Blunier, T., Dahl-Jensen, D., Ellehøj, M. D., Falourd, S., Grindsted, A., Gkinis, V., Jouzel, J., Popp, T., Sheldon, S., Simonsen, S. B., Sjolte, J., Steffensen, J. P., Sperlich, P., Sveinbjörnsdóttir, A. E., Vinther, B. M. and White, J. W. C.: Continuous monitoring of summer surface water vapor isotopic composition above the Greenland Ice Sheet, Atmos. Chem. Phys., 13(9), 4815–4828, doi:10.5194/acp-13-4815-2013, 2013.

Steen-Larsen, H. C., Masson-Delmotte, V., Hirabayashi, M., Winkler, R., Satow, K., Prié, F., Bayou, N., Brun, E., Cuffey, K. M., Dahl-Jensen, D., Dumont, M., Guillevic, M., Kipfstuhl, S., Landais, A., Popp, T., Risi, C., Steffen, K., Stenni, B. and Sveinbjörnsdottír, A. E.: What controls the isotopic composition of Greenland surface snow?, Clim. Past, 10(1), 377–392, doi:10.5194/cp-10-377-2014, 2014.

Steen-Larsen, H. C., Sveinbjörnsdottir, A. E., Jonsson, Th., Ritter, F., Bonne, J.-L., Masson-Delmotte, V., Sodemann, H., Blunier, T., Dahl-Jensen, D. and Vinther, B. M.: Moisture sources and synoptic to seasonal variability of North Atlantic water vapor isotopic composition, J. Geophys. Res. Atmos., 120(12), 2015JD023234, doi:10.1002/2015JD023234, 2015.

Steen-Larsen, H. C., Risi, C., Werner, M., Yoshimura, K. and Masson-Delmotte, V.: Evaluating the skills of isotope-enabled general circulation models against in situ atmospheric water vapor isotope observations, J. Geophys. Res. Atmos., 2016JD025443, doi:10.1002/2016JD025443, 2017.

Stohl, A., Forster, C., Frank, A., Seibert, P. and Wotawa, G.: Technical note: The Lagrangian particle dispersion model FLEXPART version 6.2, Atmos. Chem. Phys., 5(9), 2461–2474, doi:10.5194/acp-5-2461-2005, 2005.

Vihma, T., Screen, J., Tjernström, M., Newton, B., Zhang, X., Popova, V., Deser, C., Holland, M. and Prowse, T.: The atmospheric role in the Arctic water cycle: A review on processes, past and future changes, and their impacts, Journal of Geophysical Research: Biogeosciences, 586–620, doi:10.1002/2015JG003132@10.1002/(ISSN)2169-8961.FRESHWATER1, 2015.

Zannoni, D., Steen-Larsen, H. C., Stenni, B., Dreossi, G. and Rampazzo, G.: Synoptic to mesoscale processes affecting the water vapor isotopic daily cycle over a coastal lagoon, Atmospheric Environment, 197, 118–130, doi:10.1016/j.atmosenv.2018.10.032, 2019.